NATIONAL ADVISORY COMMITTEE FOR AERONAUTICS

TECHNICAL NOTE 2205

THEORETICAL SUPERSONIC CHARACTERISTICS OF INBOARD TRAILING-EDGE FLAPS HAVING ARBITRARY SWEEP AND TAPER

MACH LINES BEHIND FLAP LEADING AND TRAILING EDGES

By Julian H. Kainer and Jack E. Marte

Langley Aeronautical Laboratory
Langley Air Force Base, Va.

Washington
October 1950

NATIONAL ADVISORY COMMITTEE FOR AERONAUTICS

TECHNICAL NOTE 2205

THEORETICAL SUPERSONIC CHARACTERISTICS OF INBOARD TRAILING-EDGE FLAPS HAVING ARBITRARY SWEEP AND TAPER

MACH LINES BEHIND FLAP LEADING AND TRAILING EDGES

By Julian H. Kainer and Jack E. Marte

SUMMARY

Generalized expressions in closed form have been obtained by means of linearized theory for the aerodynamic characteristics (lift-, rolling-moment-, pitching-moment-, and hinge-moment-coefficient derivatives) due to deflection of inboard trailing-edge flaps. The analysis considers the effects of Mach number and flap aspect ratio, taper ratio, and sweep for the conditions where the Mach lines lie behind the flap leading and trailing edges. The flap configurations analyzed are limited to the case of streamwise tips where the foremost Mach lines from the flap tips do not intersect the root and tip chords of the wing. The expressions for the hinge-moment-coefficient derivative are limited to configurations where the flap-root-chord Mach line does not intersect the flap tip chord.

Design charts are presented for the rapid estimation of the characteristics due to flap deflection for control surfaces for which the Mach lines from the flap tips do not intersect on the control surface. Some illustrative variations of the characteristics with leading-edge sweep, aspect ratio, taper ratio, and Mach number are also presented.

The lift-coefficient derivative at constant Mach number is dependent only on the trailing-edge sweep; whereas the moment-coefficient derivatives depend on the complete flap geometry.

INTRODUCTION

The characteristics of control surfaces at supersonic speeds have been extensively investigated by means of linearized theory. Reference 1 presents the fundamentals of the control-surface problem; whereas a procedure for obtaining solutions for general configurations was given in reference 2. Another investigation, reference 3, presents detailed

analyses of specialized plan forms. The present paper presents the effects of sweep, aspect ratio, taper ratio, and Mach number on the lift-, rolling-moment-, pitching-moment-, and hinge-moment-coefficient derivatives of inboard trailing-edge flaps at supersonic speeds. The analysis covers a range of Mach numbers in which the leading and trailing edges of the control surfaces are supersonic (component of free-stream Mach number normal to the leading and trailing edges is greater than 1). The plan forms considered have streamwise tips, and the location of the flap on the wing is limited to cases where the foremost Mach lines from the flap tips do not intersect the root and tip chords of the wing. The analysis for the hinge-moment-coefficient derivative was limited to configurations where the flap-root-chord Mach line does not intersect the flap tip chord.

The results of the theoretical analysis, the lift, rolling-moment, pitching-moment, and hinge-moment characteristics due to flap deflection, are presented in closed-form equations as functions of sweep, taper ratio, aspect ratio, and Mach number. Design charts have been presented which permit the rapid estimation of the flap characteristics for a wide variety of configurations. Some illustrative variations of the flap characteristics with sweepback, aspect ratio, taper ratio, and Mach number are presented for representative configurations.

SYMBOLS

Free-stream conditions:

V	velocity
M	Mach number
μ	Mach angle $\left(\sin^{-1}\frac{1}{M}\right)$
$\beta = \sqrt{M^2 - 1}$	
ρ	mass density of air
q	dynamic pressure $\left(\frac{1}{2}\rho V^2\right)$

Wing geometry:

b	span
c_r	root chord

c_t tip chord

λ taper ratio (c_t/c_r)

$\bar{c}$ average chord $\left(\frac{1}{2}c_r(1 + \lambda)\right)$

Λ leading-edge sweep, degrees

S area

Control-surface geometry:

b_f span

c_{f_r} root chord

c_{f_t} tip chord

λ_f taper ratio $\left(c_{f_t}/c_{f_r}\right)$

$\bar{c}_f$ average chord $\left(\frac{1}{2}c_{f_r}(1 + \lambda_f)\right)$

c_f' root-mean-square chord

Λ_1 leading-edge sweep, degrees

Λ_2 trailing-edge sweep, degrees

$m_1 = \cot \Lambda_1$

$m_2 = \cot \Lambda_2$

$m_1' = m_1\beta$

$m_2' = m_2\beta$

S_f area

A_f aspect ratio $\left(b_f^2/S_f\right)$

$A_f' = A_f\beta$

δ deflection angle in stream direction, radians

x,y Cartesian coordinates of system of axes with origin at leading edge of control-surface root chord

x_a,y_a Cartesian coordinates of system of axes with origin at leading edge of control-surface tip chord

$\bar{x},\bar{y}$ coordinates of center of lift of infinitesimal lift triangle

$\bar{x}'$ normal distance from center of lift of infinitesimal lift triangle to hinge line

Force and moments:

L lift

L' rolling moment

M' pitching moment

H hinge moment

C_L lift coefficient $\left(L/qS_f\right)$

C_l rolling-moment coefficient $\left(L'/qb_fS_f\right)$

C_m pitching-moment coefficient $\left(M'/qb_f\bar{c}_f^2\right)$

C_h hinge-moment coefficient $\left(H/qb_f(c_f')^2\right)$

Δp pressure differential existing across surfaces of flap plate

Analysis parameters:

ϕ_x horizontal perturbation velocity

$t = \frac{\beta y}{x}$

$t_a = \frac{\beta y_a}{x_a}$

S' area of integration

Subscript:

δ refers to partial derivative of each coefficient with respect to δ; for example, $C_{L_\delta} = \frac{\partial}{\partial\delta}(C_L)$

ANALYSIS

Scope.- The analysis is based on the solution of the linearized equation for steady supersonic flow. The results are valid for a range of supersonic speeds in which the components of the free-stream velocity normal to the leading and trailing edges are supersonic. (Hereinafter these edges are referred to as supersonic leading and trailing edges.) In addition, the Mach lines from the tips of the control surface are assumed not to intersect the root and tip chords of the wing. (See fig. 1.)

Within the first order the derivatives have the same values in the stability system as in the body-axes system.

Derivation of formulas for C_{L_δ}, C_{l_δ}, C_{m_δ}, and C_{h_δ}.- In order to evaluate the derivatives C_{L_δ}, C_{l_δ}, C_{m_δ}, and C_{h_δ}, it is necessary to integrate over the appropriate areas the pressures caused by the disturbances induced by the deflected flap, which within the limits of the linearized theory may be treated as a flat plate. Thus, the derivative C_{L_δ} is obtained by integrating $\Delta p/q$ over the area supporting the lift forces and then taking the derivative of the lift coefficient with respect to δ. Similarly, the moment derivatives are obtained by considering the respective moments due to the lifts over the proper areas. Since the lifts and moments vary linearly with respect to δ, the desired quantities may be expressed as follows:

$$\left.\begin{aligned} C_{L_\delta} &= \frac{1}{S_f}\int \frac{\Delta p}{q\delta}\,dS' \\ C_{l_\delta} &= \frac{1}{S_f}\int \frac{y}{b_f}\frac{\Delta p}{q\delta}\,dS' \\ C_{m_\delta} &= \frac{1}{S_f}\int \frac{\bar{x}}{\bar{c}_f}\frac{\Delta p}{q\delta}\,dS' \\ C_{h_\delta} &= \frac{1}{S_f}\int \frac{\bar{x}'}{\bar{c}_f}\left(\frac{\bar{c}_f}{c_f'}\right)^2\frac{\Delta p}{q\delta}\,dS' \end{aligned}\right\} \qquad (1)$$

where the integration for the first three characteristics includes the regions (OAB and O'B'C' of fig. 2) on the wing supporting the lifts induced by the interference between the control surface and the wing. The induced lifts on these regions contribute no hinge moment and, hence, are not included in the derivation of C_{h_δ}.

Pressure distributions.- The pressure differential across the surface of a deflected flat plate is

$$\frac{\Delta p}{q} = -\frac{4}{V}\phi_x \tag{2}$$

where ϕ_x is the perturbation velocity in the x-direction. The pressure distributions for the control surfaces, which can be treated as lifting wings of finite aspect ratio, were obtained with the use of the methods of references 4 and 5. The deflected flap was superposed on a wing at zero angle of attack. (See reference 1 and fig. 1 of present paper.) The control surface is shown in figure 2 isolated from the wing. Since the foremost Mach lines from the tips of the control surface intersect the trailing edge of the adjacent wing (fig. 1), the disturbances within the root and tip Mach cones are similar, and the discussion may be limited to either one.

When the control surface is deflected with respect to the wing at zero angle of attack, an interference between the wing and flap takes place within the Mach cone with its apex at point O of figure 2. The gap between the deflected flap and the wing is assumed to be sealed completely; therefore, one surface is prevented from affecting the other. The pressure distributions may be obtained in the manner of reference 4 or 5 and are presented in table I.

The conical form of the equations for $\Delta p/q\delta$ suggests the use of polar integration for obtaining the characteristics. The derivation of C_{m_δ} is given in the appendix as an example of this use of polar integration; illustrative data for the integration are given in figure 2.

Control-surface parameters.- The expressions for the contributions of each region (fig. 1) to βC_{L_δ}, βC_{l_δ}, βC_{m_δ}, and $\left(\frac{c_f'}{c_f}\right)^2 \beta \sec \Lambda_1 C_{h_\delta}$ are presented in tables II to V, respectively. The following expressions are for the deflection of one flap when the foremost Mach lines from the tips of the flap are assumed to intersect the trailing edge of the adjacent wing surface:

$$\beta C_{L_\delta} = \beta\left(C_{L_\delta}\right)_{OAC'} + \beta\left(C_{L_\delta}\right)_{O'A'C'} + \beta\left(C_{L_\delta}\right)_{\infty} \tag{3}$$

$$\beta C_{l_\delta} = \beta\left(C_{l_\delta}\right)_{OAC} + \beta\left(C_{l_\delta}\right)_{O'A'C'} + \beta\left(C_{l_\delta}\right)_{\infty} \tag{4}$$

$$\beta C_{m_\delta} = \beta\left(C_{m_\delta}\right)_{OAC} + \beta\left(C_{m_\delta}\right)_{O'A'C'} + \beta\left(C_{m_\delta}\right)_{\infty} \tag{5}$$

$$\left(\frac{c_f'}{\bar{c}_f}\right)^2 \beta \sec \Lambda_1 C_{h_\delta} = \left[\beta \sec \Lambda_1\left(C_{h_\delta}\right)_{OBC} + \beta \sec \Lambda_1\left(C_{h_\delta}\right)_{O'A'B'} + \beta \sec \Lambda_1\left(C_{h_\delta}\right)_{\infty}\right]\left(\frac{c_f'}{\bar{c}_f}\right)^2 \tag{6}$$

The rolling-moment- and pitching-moment-coefficient derivatives have been obtained about the axes of a Cartesian coordinate system located at the leading edge of the root chord of the flap (fig. 2) and may be transferred to any convenient reference axes by

$$\beta C_{l_\delta}{}^* = \beta C_{l_\delta} + \frac{y}{b_f}\beta C_{L_\delta} \tag{7}$$

$$\beta C_{m_\delta}{}^* = \beta C_{m_\delta} + \frac{2}{1 + \lambda_f}\frac{x}{c_{f_r}}\beta C_{L_\delta} \tag{8}$$

where the asterisked characteristics in equations (7) and (8) refer to the transferred quantities, and x and y represent the horizontal and vertical distances between the present axes and the desired ones.

The quantities in equations (3) to (6) were made nondimensional by the use of control-surface parameters. Equations (3) to (5) may be defined in terms of wing parameters with the use of the following equations:

$$\frac{S_f}{S} = \frac{b_f}{b}\frac{c_{f_r}}{c_r}\frac{1 + \lambda_f}{1 + \lambda} \tag{9}$$

$$\frac{b_f S_f}{bS} = \left(\frac{b_f}{b}\right)^2 \frac{c_{f_r}}{c_r}\frac{1 + \lambda_f}{1 + \lambda} \tag{10}$$

$$\frac{\bar{c}_f S_f}{\bar{c}S} = \frac{b_f}{b}\left(\frac{c_{f_r}}{c_r}\right)^2\left(\frac{1 + \lambda_f}{1 + \lambda}\right)^2 \tag{11}$$

where equations (3) to (5) are multiplied by equations (9) to (11), respectively. The area S_f is the area of one flap and S is the entire area of the wing.

DISCUSSION

Generalized expressions in closed form, which were obtained by means of linearized theory, are presented for the characteristics of deflected inboard trailing-edge control surfaces βC_{L_δ}, βC_{l_δ}, βC_{m_δ}, and $\left(\frac{c_f'}{\bar{c}_f}\right)^2 \sec \Lambda_1 \, C_{h_\delta}$ in tables II to V, respectively. The control surfaces have arbitrary sweep, aspect ratio, and taper and the Mach lines are behind the control-surface leading and trailing edges. The expressions for the hinge-moment-coefficient parameter are limited to configurations where the root-chord Mach line does not intersect the flap tip chord, that is, $m_1' \geqq \frac{1}{1 - \frac{2\lambda_f}{A_f'(1 + \lambda_f)}}$. Design charts are presented in figures 3 to 14 for configurations where the Mach lines from the control-surface tips do not intersect on the flap. In the vicinity of the sonic leading edge $(\beta \cot \Lambda_1 = 1)$, βC_{L_δ}, βC_{l_δ}, and βC_{m_δ} have finite values which increase with taper ratio and become infinite for an untapered configuration. The large values associated with the less-tapered configurations are attributed to the large lift carry-over region which occurs for the wing-flap configurations which are within the scope of the present paper. The parameter βC_{L_δ} and, hence, βC_{l_δ} and βC_{m_δ} become infinite for configurations having sonic trailing edges $(\beta \cot \Lambda_2 = 1)$ since the lift carry-over region becomes infinite. Since the carry-over regions on actual configurations are small, the large values of βC_{L_δ}, βC_{l_δ}, and βC_{m_δ} predicted in the vicinity of the sonic leading and trailing edges will not be realized. The hinge-moment-coefficient parameter remains finite for both sonic leading and trailing edges since the lift carry-over regions do not contribute any hinge moment.

Figure 3 presents the variation of βC_{L_δ} with $|\beta \cot \Lambda_2|$. The nature of βC_{L_δ} (dependent only on $\beta \cot \Lambda_2$) is due to the interference on the control surface (reference 1). No leakage is assumed to occur through the gap between the wing and the control surface. The loss in lift within the tip Mach cone on the flap is reduced; whereas

an induced lift is supported within the Mach cone on the wing. The induced lift compensates the loss of lift on untapered flaps only.

The solution for βC_{L_δ} as a function of $\beta \cot \Lambda_2$ may be more easily obtained from equation (1) by integrating the velocity potential evaluated at the trailing edge in the manner of reference 6.

Figures 4 to 6 present the variations of the rolling-moment-, pitching-moment-, and hinge-moment-coefficient parameters, βC_{l_δ}, βC_{m_δ}, $\left(\frac{c_f'}{\bar{c}_f}\right)^2 \beta \sec \Lambda_1 \, C_{h_\delta}$, respectively, with $\beta \cot \Lambda_1$ for several families of $A_f\beta$ and λ_f.

Figures 11 to 14 give some illustrative variations of C_{L_δ}, C_{l_δ}, C_{m_δ}, and $\left(\frac{c_f'}{\bar{c}_f}\right)^2 C_{h_\delta}$, respectively, with Mach number, aspect ratio, leading-edge sweep, and taper ratio.

CONCLUDING REMARKS

Generalized expressions in closed form have been obtained by means of linearized theory for the aerodynamic characteristics due to deflection of inboard trailing-edge flaps. The analysis considers the effects of Mach number and flap aspect ratio, taper ratio, and sweep for the conditions where the Mach lines lie behind the flap leading and trailing edges. The flap configurations analyzed are limited to the case of streamwise tips where the foremost Mach lines from the flap tips do not intersect the root and tip chords of the wing. The expressions for the hinge-moment-coefficient derivative are limited to configurations where the flap-root-chord Mach line does not intersect the flap tip chord.

Design charts are presented for the rapid estimation of the aerodynamic characteristics due to flap deflection for configurations for which the Mach lines from the flap tips do not intersect on the control surface. Some illustrative variations of the characteristics with leading-edge sweep, aspect ratio, taper ratio, and Mach number are also presented.

The lift-coefficient derivative at constant Mach number is dependent only on the trailing-edge sweep; whereas the moment-coefficient derivatives depend on the complete flap geometry.

The general expressions and curves were expressed in terms of control-surface parameters; formulas are given for converting all characteristics to wing parameters.

Langley Aeronautical Laboratory
National Advisory Committee for Aeronautics
Langley Air Force Base, Va., August 7, 1950

APPENDIX

DETAILS OF POLAR INTEGRATION; DERIVATION OF C_{m_δ} AS AN EXAMPLE

The pitching-moment derivative C_{m_δ} is derived by polar integration as an example of the manner in which the characteristics due to flap deflection were obtained.

The lift on an infinitesimal triangle (fig. 2) is assumed to be constant; therefore, the center of pressure (or lift) is located at

$$\left.\begin{aligned} \bar{x} &= \frac{2}{3}x \\ \bar{y} &= \frac{\bar{x}}{\beta}t \end{aligned}\right\} \tag{A1}$$

where

$$t = \frac{\beta y}{x} \tag{A2}$$

The area of the infinitesimal triangle may be shown to be

$$dS' = \frac{1}{2}x\,dy = \frac{1}{2\beta}x^2 dt \tag{A3}$$

If the equation of the trailing edge is written as

$$y = m_2\left(x - c_{f_r}\right) \tag{A4}$$

then with the use of equation (A2) the following equation can be written:

$$x = \frac{m_2' c_{f_r}}{m_2' - t} \tag{A5}$$

Hence,

$$dS' = \frac{\left(m_2'\right)^2 c_{f_r}^{\,2}}{2\beta} \frac{dt}{\left(m_2' - t\right)^2} \tag{A6}$$

The moment arms of any point (x,y) or any value of t are $\bar{x}$ for pitching moment, $\bar{y}$ for rolling moment, and $\bar{x}'$ for hinge moment. These moment arms, written in terms of t, are

$$\bar{x} = \frac{2m_2' c_{f_r}}{3(m_2' - t)} \tag{A7}$$

$$\bar{y} = \frac{2m_2' c_{f_r}}{3\beta} \frac{t}{m_2' - t} \tag{A8}$$

$$\bar{x}' = \left(\bar{x} - \frac{\bar{y}}{m_1}\right)\cos \Lambda_1 = \frac{2m_2' c_{f_r} \cos \Lambda_1}{3m_1} \frac{m_1' - t}{m_2' - t} \tag{A9}$$

where the equations (A1) to (A9) refer to the region OAC. The equations for region O'A'C' are obtained by replacing t by t_a in the respective equations, where

$$t_a = \frac{\beta y_a}{x_a} \tag{A10}$$

The pitching-moment coefficient in region OAC, given generally by equation (1) of the text, is

$$C_{m_\delta} = \frac{1}{\bar{c}_f S_f} \int_{OAC} \bar{x} \frac{\Delta p}{q\delta} \, dS' \tag{A11}$$

$$C_{m_\delta} = \frac{4m_1'(m_2')^3 c_{f_r}^3}{3\pi\beta^2 \bar{c}_f S_f \sqrt{(m_1')^2 - 1}} \int_{t=-1}^{t=1} \left(\frac{1}{m_2' - t}\right)^3 \cos^{-1} \frac{1 - m_1' t}{m_1' - t} \, dt \tag{A12}$$

Integration by parts gives

$$\beta(C_{m_\delta})_{OAC} = \frac{16m_1'(m_2')^3}{3\pi A_f'(1+\lambda_f)^3\sqrt{(m_1')^2-1}}\left[\frac{\cos^{-1}\frac{1-m_1't}{m_1'-t}}{(m_2'-t)^2}+\frac{\sqrt{(m_1')^2-t}}{m_1'-m_2'}\left\{\frac{\sqrt{1-t^2}}{\left[(m_2')^2-1\right](m_2'-t)}+\right.\right.$$

$$\left.\left.\frac{m_2'}{\left[(m_2')^2-1\right]^{3/2}}\sin^{-1}\frac{1-m_2't}{t-m_2'}-\frac{1}{m_1'+m_2'}\left[\frac{\sin^{-1}\frac{1-m_2't}{t-m_2'}}{\sqrt{(m_2')^2-1}}-\frac{\sin^{-1}\frac{1-m_1't}{t-m_1'}}{\sqrt{(m_1')^2-1}}\right]\right\}\right]_{-1}^{1} \tag{A13}$$

$$\beta(C_{m_\delta})_{OAC} = \frac{16m_1'(m_2')^3}{3A_f'(1+\lambda_f)^3\sqrt{(m_1')^2-1}}\left\{\left(\frac{1}{m_2'-1}\right)^2-\frac{m_2'\sqrt{(m_1')^2-1}}{(m_1'-m_2')\left[(m_2')^2-1\right]^{3/2}}+\right.$$

$$\left.\left(\frac{1}{m_1'+m_2'}\right)^2\left(\sqrt{\frac{(m_1')^2-1}{(m_2')^2-1}}-1\right)\right\} \tag{A14}$$

The corresponding formulas for the region O'A'C' may be obtained in the same manner or by simply changing the signs of m_1' and m_2' and inverting the taper ratio in the formulas for the region OAC. When m_1' or m_2' is negative, the negative square roots should be used.

REFERENCES

1. Lagerstrom, P. A., and Graham, Martha E.: Linearized Theory of Supersonic Control Surfaces. Jour. Aero. Sci., vol. 16, no. 1, Jan. 1949, pp. 31-34.

2. Frick, Charles W., Jr.: Application of the Linearized Theory of Supersonic Flow to the Estimation of Control-Surface Characteristics. NACA TN 1554, 1948.

3. Tucker, Warren A., and Nelson, Robert L.: Theoretical Characteristics in Supersonic Flow of Two Types of Control Surfaces on Triangular Wings. NACA Rep. 939, 1949.

4. Puckett, Allen E.: Supersonic Wave Drag of Thin Airfoils. Jour. Aero. Sci., vol. 13, no. 9, Sept. 1946, pp. 475-484.

5. Jones, Robert T.: Thin Oblique Airfoils at Supersonic Speed. NACA Rep. 851, 1946.

6. Harmon, Sidney M., and Jeffreys, Isabella: Theoretical Lift and Damping in Roll of Thin Wings with Arbitrary Sweep and Taper at Supersonic Speeds. Supersonic Leading and Trailing Edges. NACA TN 2114, 1950.

TABLE I.- GENERALIZED FORMULAS FOR $\Delta p/q$ DISTRIBUTIONS FOR A CONTROL SURFACE AT CONSTANT DEFLECTION ANGLE δ

$$\left[\beta \cot \Lambda_1 > 1;\ \left|\beta \cot \Lambda_2\right| \gtrless 1;\ m_2' = \frac{1}{\frac{1}{m_1'} - \frac{2(1-\lambda_f)}{A_f'(1+\lambda_f)}}\right]$$

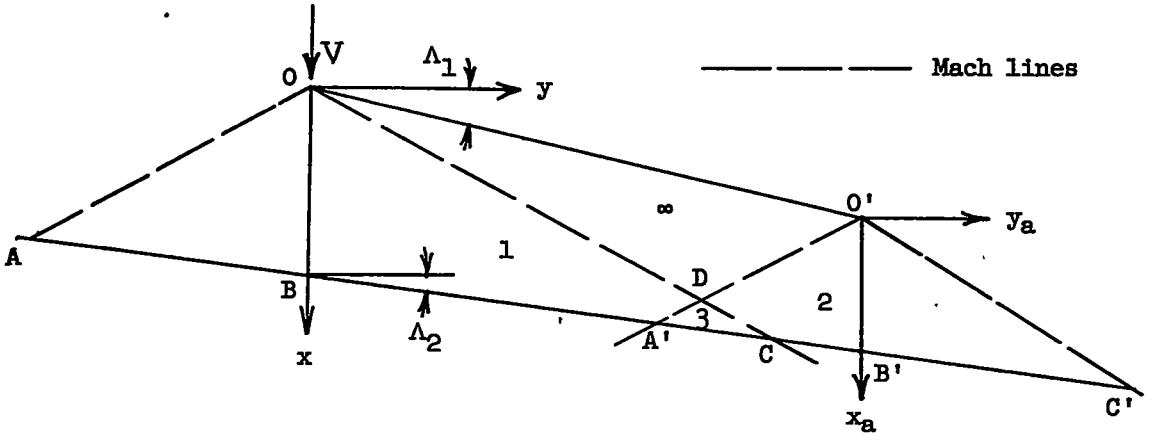

Region (See sketch)	Formulas for $\Delta p/q$ contributed by constant δ
∞	$\dfrac{4\delta m_1}{\sqrt{(m_1')^2 - 1}}$
1	$\dfrac{4\delta m_1}{\pi\sqrt{(m_1')^2 - 1}} \cos^{-1} \dfrac{x - m_1'\beta y}{m_1' x - \beta y}$
2	$\dfrac{4\delta m_1}{\pi\sqrt{(m_1')^2 - 1}} \cos^{-1} - \dfrac{x_a - m_1'\beta y_a}{m_1' x_a - \beta y_a}$
3	$\left(\dfrac{\Delta p}{q}\right)_1 + \left(\dfrac{\Delta p}{q}\right)_2 - \left(\dfrac{\Delta p}{q}\right)_\infty$

NACA

TABLE II.- GENERALIZED FORMULAS FOR βC_{l_δ}

$\left[\beta \cot \Lambda_1 > 1;\ \left|\beta \cot \Lambda_2\right| \geq 1\right]$

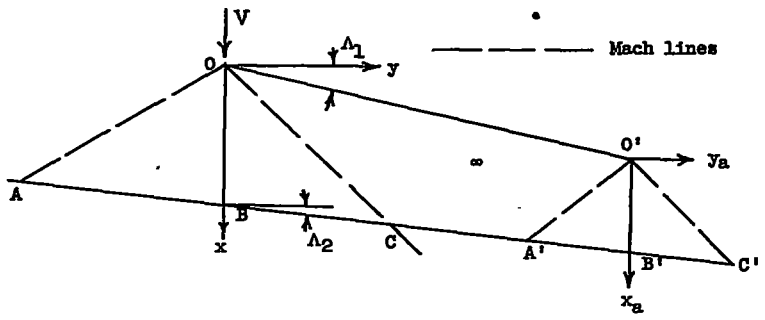

Region (See sketch)	Formulas for βC_{l_δ}
Tapered; $m_1' \neq \infty$; $m_2' \neq \infty$	
OAC	$\frac{8m_1'(m_2')^2}{A_f'(1+\lambda_f)^2\sqrt{(m_1')^2-1}}\left\{\left(\frac{1}{m_1'-m_2'}\right)\left[\frac{m_1'-1}{m_2'-1}-\sqrt{\frac{(m_1')^2-1}{(m_2')^2-1}}\right]\right\}$
O'A'C'	$\frac{16m_1'(m_2')^2\lambda_f^2}{A_f'(1+\lambda_f)^2\sqrt{(m_1')^2-1}}\left[\frac{1}{(m_2')^2-1}\right]-\lambda_f^2\left(\beta C_{l_\delta}\right)_{OAC}$
∞	$\frac{8m_1'}{A_f'(1+\lambda_f)^2\sqrt{(m_1')^2-1}}\left\{\left[\frac{(m_2')^2}{(m_2')^2-1}\right]\left[\frac{A_f'}{2}(1+\lambda_f)\left(1+\frac{1}{m_1'}\right)\left(1-\frac{1}{m_2'}\right)-2\right]+\frac{A_f'(1+\lambda_f)\left(1+\frac{1}{m_1'}\right)\lambda_f}{2\left(1+\frac{1}{m_2'}\right)}\right\}$
Total	$4m_2'/\sqrt{(m_2')^2-1}$
Untapered; $m' \neq \infty$	
OAC	$\frac{2(m')^3}{A_f'\left[(m')^2-1\right]^{3/2}}$
O'A'C'	$\frac{2(m')^3}{A_f'\left[(m')^2-1\right]^{3/2}}$
∞	$\frac{4m'}{A_f'\sqrt{(m')^2-1}}\left[A_f'-\frac{(m')^2}{(m')^2-1}\right]$
Total	$4m'/\sqrt{(m')^2-1}$
$m' = \infty$	
OAC	$2/A_f'$
O'A'C'	$2/A_f'$
∞	$4\left(1-\frac{1}{A_f'}\right)$
Total	4

NACA

TABLE III.- GENERALIZED FORMULAS FOR βC_{l_δ}

$\left[\beta \cot \Lambda_1 > 1;\ \left|\beta \cot \Lambda_2\right| \geq 1\right]$

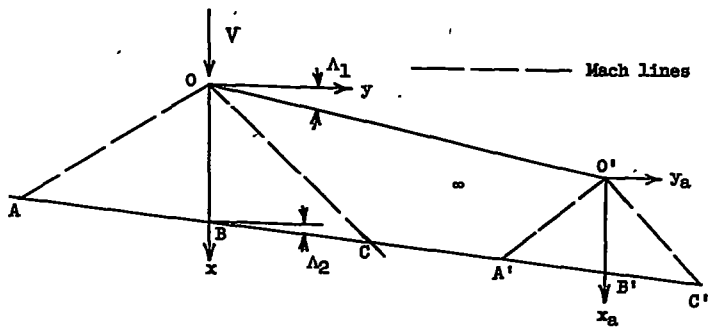

Region (See sketch)	Formulas for βC_{l_δ}
Tapered; $m_1' \neq \infty$; $m_2' \neq \infty$	
OAC	$\frac{32m_1'(m_2')^3}{3(A_f')^2(1+\lambda_f)^3\sqrt{(m_1')^2-1}}\left\{\left[\frac{m_2'}{2(m_2'-1)}-1\right]\frac{1}{m_2'-1}-\frac{(m_2')^2\sqrt{(m_1')^2-1}}{2(m_1'-m_2')\left[(m_2')^2-1\right]^{3/2}}+\left(\frac{1}{m_1'-m_2'}\right)\left[\frac{m_2'}{2(m_1'-m_2')}+1\right]\left[\sqrt{\frac{(m_1')^2-1}{(m_2')^2-1}}-1\right]\right\}$
O'A'C'	$\frac{64m_1'(m_2')^3\lambda_f^3}{3(A_f')^2(1+\lambda_f)^3\sqrt{(m_1')^2-1}\left[(m_2')^2-1\right]^2}-\lambda_f^3\left(\beta C_{l_\delta}\right)_{OAC}+\left(\beta C_{l_\delta}\right)_{O'A'C'}$
∞	$\frac{16m_1'}{3(A_f')^2(1+\lambda_f)^3\sqrt{(m_1')^2-1}}\left\{\left(1+\frac{1}{m_1'}\right)\left[\frac{1}{2}A_f'(1+\lambda_f)\right]^3-\left(\frac{m_2'}{m_2'-1}\right)^2-\left(\frac{m_2'}{m_2'+1}\right)^2\left[\frac{1}{2}A_f'(1+\lambda_f)\left(1+\frac{1}{m_1'}\right)-1\right]^3\right\}$
Untapered; $m' \neq \infty$	
OAC	$\frac{(m')^4(m'+4)}{3(A_f')^2\left[(m')^2-1\right]^{5/2}}$
O'A'C'	$\frac{8(m')^4}{3(A_f')^2\left[(m')^2-1\right]^{5/2}}-\left[\left(\beta C_{l_\delta}\right)_{OAC}\right]_{\lambda_f=1}+\left[\left(\beta C_{l_\delta}\right)_{O'A'C'}\right]_{\lambda_f=1}$
∞	$\frac{2m'}{3A_f'\sqrt{(m')^2-1}}\left\{\left(1+\frac{1}{m'}\right)(A_f')^3-\left(\frac{m'}{m'-1}\right)^2-\left(\frac{m'}{m'+1}\right)^2\left[\left(1+\frac{1}{m'}\right)A_f'-1\right]^3\right\}$
$m' = \infty$	
OAC	$1/3(A_f')^2$
O'A'C'	$\frac{1}{A_f'}\left(2-\frac{1}{3A_f'}\right)$
∞	$2\left(1-\frac{1}{A_f'}\right)$
Total	2

NACA

TABLE IV.- GENERALIZED FORMULAS FOR βC_{m_δ}

$[\beta \cot \Lambda_1 > 1; |\beta \cot \Lambda_2| \gtrless 1]$

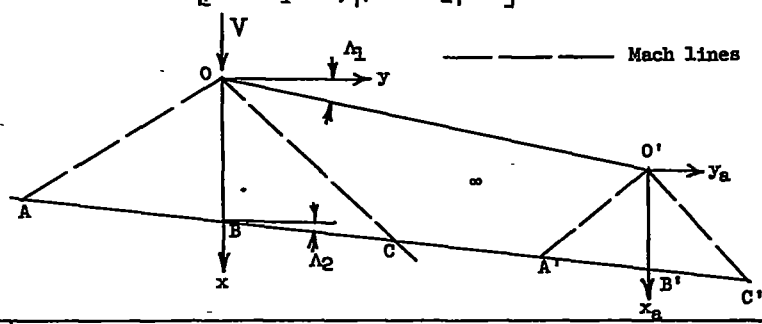

Region (See sketch)	Formulas for βC_{m_δ}
Tapered; $m_1' \neq \infty$; $m_2' \neq \infty$	
OAC	$\frac{16m_1'(m_2')^3}{3A_f'(1+\lambda_f)^3\sqrt{(m_1')^2-1}}\left\{\left(\frac{1}{m_2'-1}\right)^2 - \frac{m_2'\sqrt{(m_1')^2-1}}{(m_1'-m_2')\left[(m_2')^2-1\right]^{3/2}} + \left(\frac{1}{m_1'-m_2'}\right)^2\left[\sqrt{\frac{(m_1')^2-1}{(m_2')^2-1}}-1\right]\right\}$
O'A'C'	$\frac{64m_1'(m_2')^4\lambda_f^3}{3A_f'(1+\lambda_f)^3\sqrt{(m_1')^2-1}}\left[\frac{1}{(m_2')^2-1}\right]^2 - \lambda_f^3(\beta C_{m_\delta})_{OAC} + \frac{A_f'}{m_1'}(\beta C_{l_\delta})_{O'A'C'}$
∞	$\frac{16m_1'}{3A_f'(1+\lambda_f)^3\sqrt{(m_1')^2-1}}\left\{\frac{(m_2')^3}{(m_2'+1)^2}\left[\frac{A_f'(1+\lambda_f)}{2m_2'}\left(1+\frac{1}{m_1'}\right)+1\right]^3 - \frac{(m_2')^3}{(m_2'-1)^2} - (m_1'+1)\left[\frac{A_f'(1+\lambda_f)}{2m_1'}\right]^3\right\}$
Untapered; $m' \neq \infty$	
OAC	$\frac{(m')^4(4m'+1)}{3A_f'\left[(m')^2-1\right]^{5/2}}$
O'A'C'	$\frac{\cdot 8(m')^5}{3A_f'\left[(m')^2-1\right]^{5/2}} - \left[(\beta C_{m_\delta})_{OAC}\right]_{\lambda_f=1} + \frac{A_f'}{m'}\left[(\beta C_{l_\delta})_{O'A'C'}\right]_{\lambda_f=1}$
∞	$\frac{2m'}{3A_f'\sqrt{(m')^2-1}}\left(\frac{(m')^3}{(m'+1)^2}\left\{A_f'\left[\frac{m'+1}{(m')^2}\right]+1\right\}^3 - \frac{(m')^3}{(m'-1)^2} - (A_f')^3\left(\frac{m'+1}{(m')^3}\right)\right)$
$m' = \infty$	
OAC	$4/3A_f'$
O'A'C'	$4/3A_f'$
∞	$\frac{2}{A_f'}\left(A_f' - \frac{4}{3}\right)$
Total	2

NACA

TABLE V.- GENERALIZED FORMULAS FOR $\left(\frac{c_r'}{\bar{c}_r}\right)^2 \beta \sec \Lambda_1 C_{h_\delta}$

$[\beta \cot \Lambda_1 > 1;\ |\beta \cot \Lambda_2| \geq 1]$

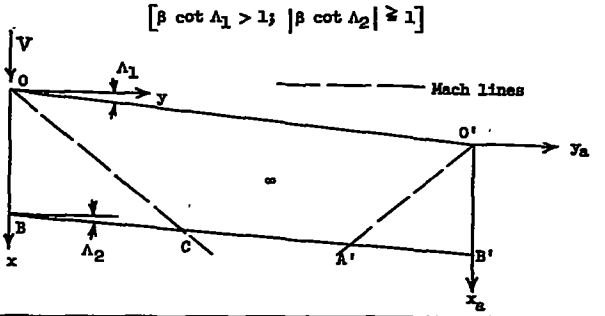

Region (See sketch)	Formulas for $\left(\frac{c_r'}{\bar{c}_r}\right)^2 \beta \sec \Lambda_1 C_{h_\delta}$
Tapered; $m_1' \neq \infty$; $m_2' \neq \infty$	
OBC	$\frac{16(m_2')^3}{3\pi A_r'(1+\lambda_r)^3\sqrt{(m_1')^2-1}}\left(\left(\frac{m_1'-m_2'}{m_2'-1}+2\right)\frac{\pi}{m_2'-1}-\frac{m_1'+m_2'}{(m_2')^2}\cos^{-1}(1/m_1')-\frac{\sqrt{(m_1')^2-1}}{m_1'-m_2'}\left[\frac{m_1'-m_2'}{m_2'\left[(m_2')^2-1\right]}+\frac{m_1'm_2'-1}{\left[(m_2')^2-1\right]^{3/2}}\cos^{-1}\left(-1/m_2'\right)-\frac{\cos^{-1}(-1/m_1')}{\sqrt{(m_1')^2-1}}\right]\right)$
O'A'B'	$\frac{16(m_2')^3\lambda_r^3}{3\pi A_r'(1+\lambda_r)^3\sqrt{(m_1')^2-1}}\left(\frac{m_1'+m_2'}{(m_2')^2}\cos^{-1}(-1/m_1')-\left(\frac{m_1'-m_2'}{m_2'+1}+2\right)\frac{\pi}{m_2'+1}-\frac{\sqrt{(m_1')^2-1}}{m_1'-m_2'}\left[\frac{m_1'-m_2'}{m_2'\left[(m_2')^2-1\right]}-\frac{m_1'm_2'-1}{\left[(m_2')^2-1\right]^{3/2}}\cos^{-1}(1/m_2')+\frac{\cos^{-1}(1/m_1')}{\sqrt{(m_1')^2-1}}\right]\right)$
∞	$\frac{16m_1'}{3A_r'(1+\lambda_r)^3\sqrt{(m_1')^2-1}}\left\{\frac{(m_2')^3}{(m_2'+1)^2}\left[\frac{A_r'(1+\lambda_r)}{2m_2'}\left(1+\frac{1}{m_1'}\right)+1\right]^3-\frac{(m_2')^3}{(m_2'-1)^2}+\frac{1}{m_1'}\left(\frac{m_2'}{m_2'-1}\right)^2-(m_1'+1)^2\left[\frac{A_r'(1+\lambda_r)}{2m_1'}\right]^3+\frac{1}{m_1'}\left(\frac{m_2'}{m_2'+1}\right)^2\left[\frac{A_r'(1+\lambda_r)}{2}\left(1+\frac{1}{m_1'}\right)-1\right]^3\right\}$
Untapered; $m' \neq \infty$	
OBC	$\frac{4(m')^3}{3\pi A_r'\left[(m')^2-1\right]^{3/2}}\left[\pi-\frac{\sqrt{(m')^2-1}}{m'}+\frac{1}{m'}\cos^{-1}(1/m')\right]$
O'A'B'	$\frac{4(m')^3}{3\pi A_r'\left[(m')^2-1\right]^{3/2}}\left[\pi-\frac{\sqrt{(m')^2-1}}{m'}-\frac{1}{m'}\cos^{-1}(-1/m')\right]$
∞	$\frac{2m'}{3A_r'\sqrt{(m')^2-1}}\left(\frac{(m')^3}{(m'+1)^2}\left[A_r'\left[\frac{m'+1}{(m')^2}\right]+1\right]^3-\frac{m'(m'+1)}{m'-1}-\frac{(m'+1)^2(A_r')^3}{(m')^3}+\frac{m'}{(m'+1)^2}\left[A_r'\left(1+\frac{1}{m'}\right)-1\right]^3\right)$
$m' = \infty$	
OBC	$\frac{4}{3\pi A_r'}(\pi-1)$
O'A'B'	$\frac{4}{3\pi A_r'}(\pi-1)$
∞	$\frac{4}{A_r'}\left(\frac{A_r'}{2}-\frac{2}{3}\right)$
Total	$2-\frac{8}{3\pi A_r'}$

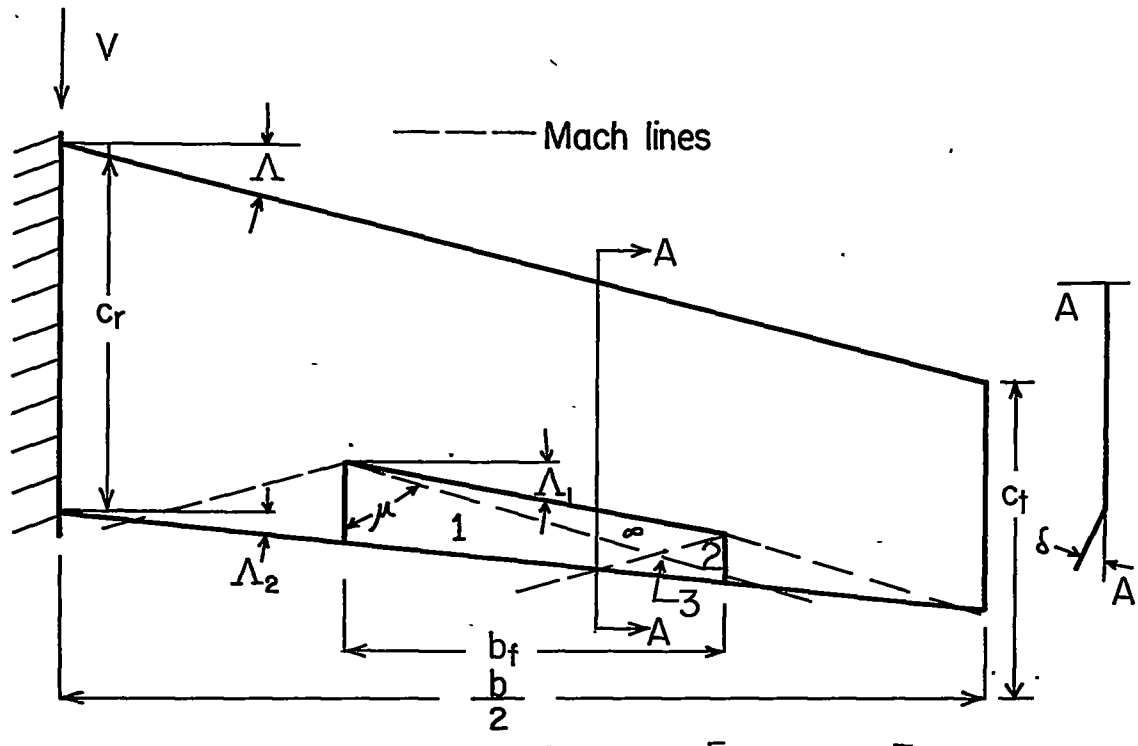

(a) $\frac{A_f'(1+\lambda_f)}{4}\left(1+\frac{1}{m_1'}\right) \leqq \frac{A_f'(1+\lambda_f)}{4}\left(1+\frac{1}{m_1'}\right)\left[\frac{1}{m_1'}-\frac{2(1-\lambda_f)}{A_f'(1+\lambda_f)}\right]+1$

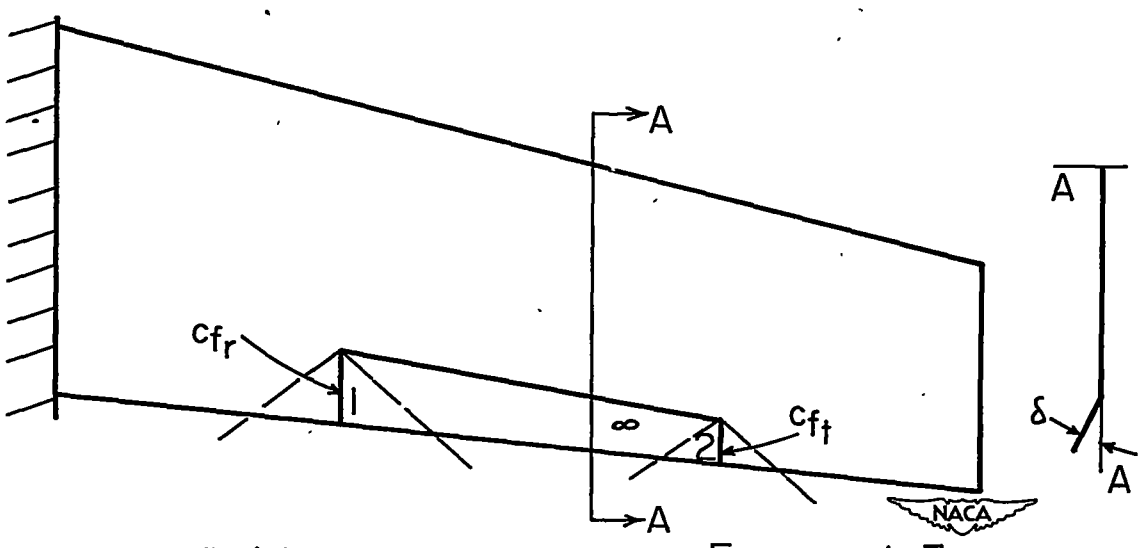

(b) $\frac{A_f'(1+\lambda_f)}{4}\left(1+\frac{1}{m_1'}\right) \geqq \frac{A_f'(1+\lambda_f)}{4}\left(1+\frac{1}{m_1'}\right)\left[\frac{1}{m_1'}-\frac{2(1-\lambda_f)}{A_f'(1+\lambda_f)}\right]+1$

Figure 1.- Typical configuration of wing with control surface.

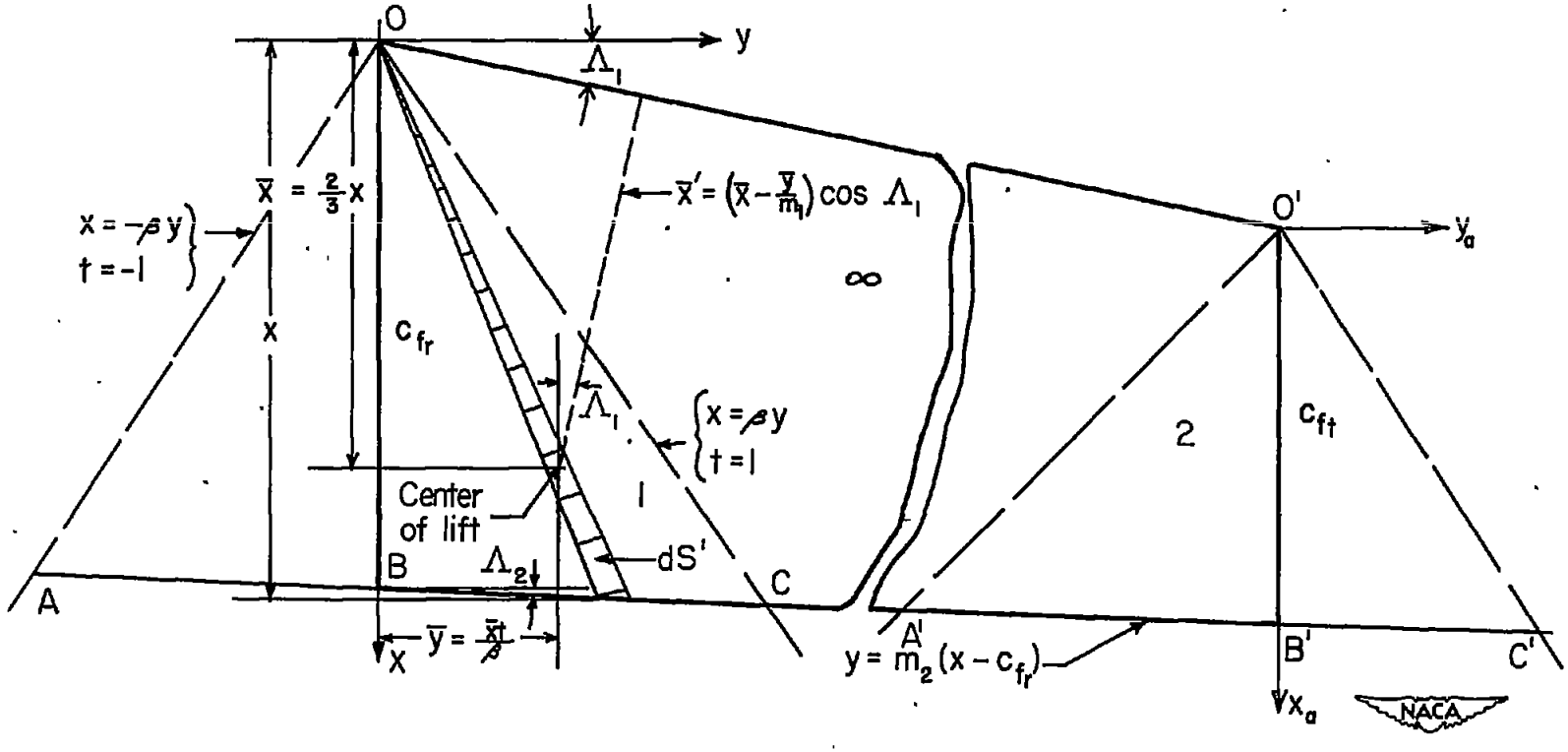

Figure 2.- Illustrative data for polar integration.

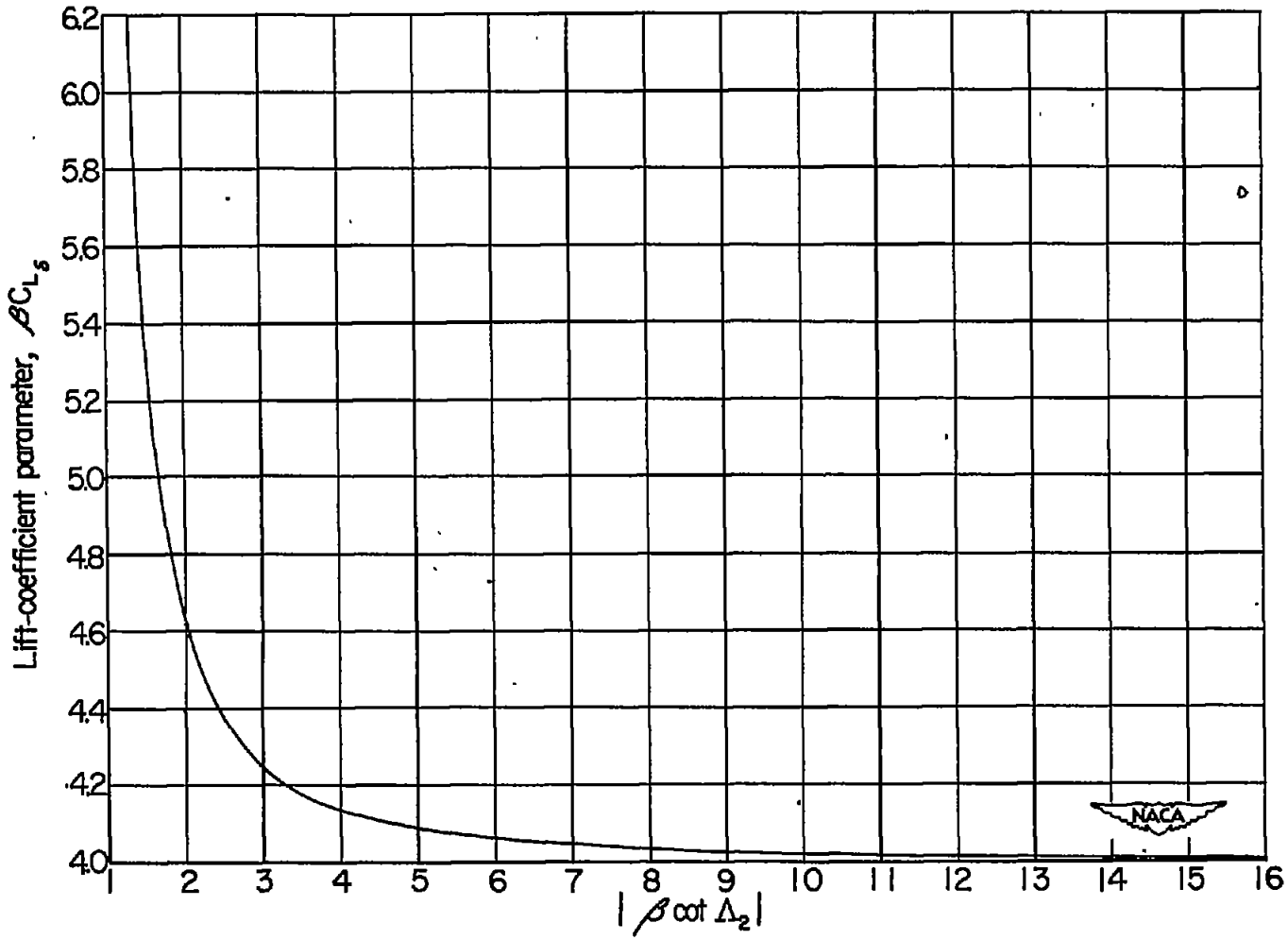

Figure 3.- Variation of βC_{L_δ} with $|\beta \cot \Lambda_2|$ for all $A_f\beta$, λ_f, and $\beta \cot \Lambda_1$.

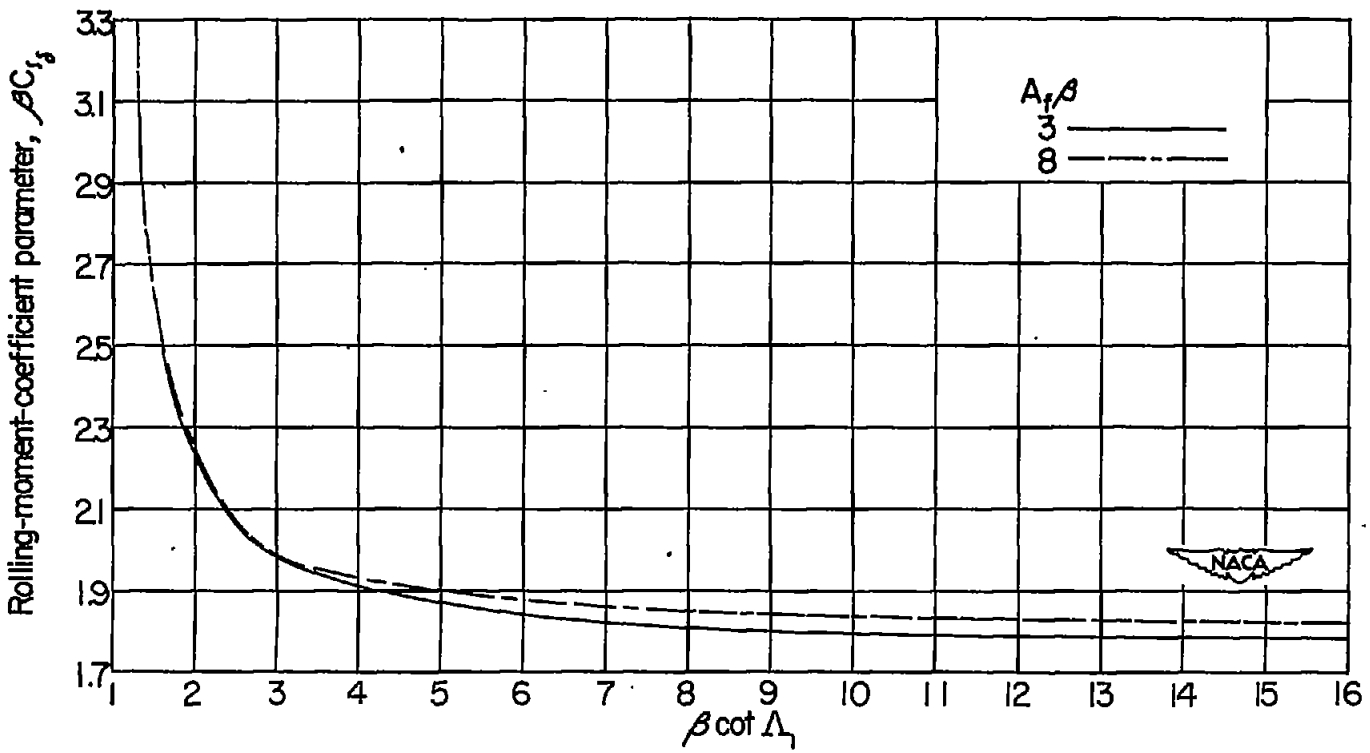

(a) $\lambda_f = 0.6$.

Figure 4.- Variation of βC_{l_δ} with $\beta \cot \Lambda_1$ for several families of $A_f\beta$ and λ_f.

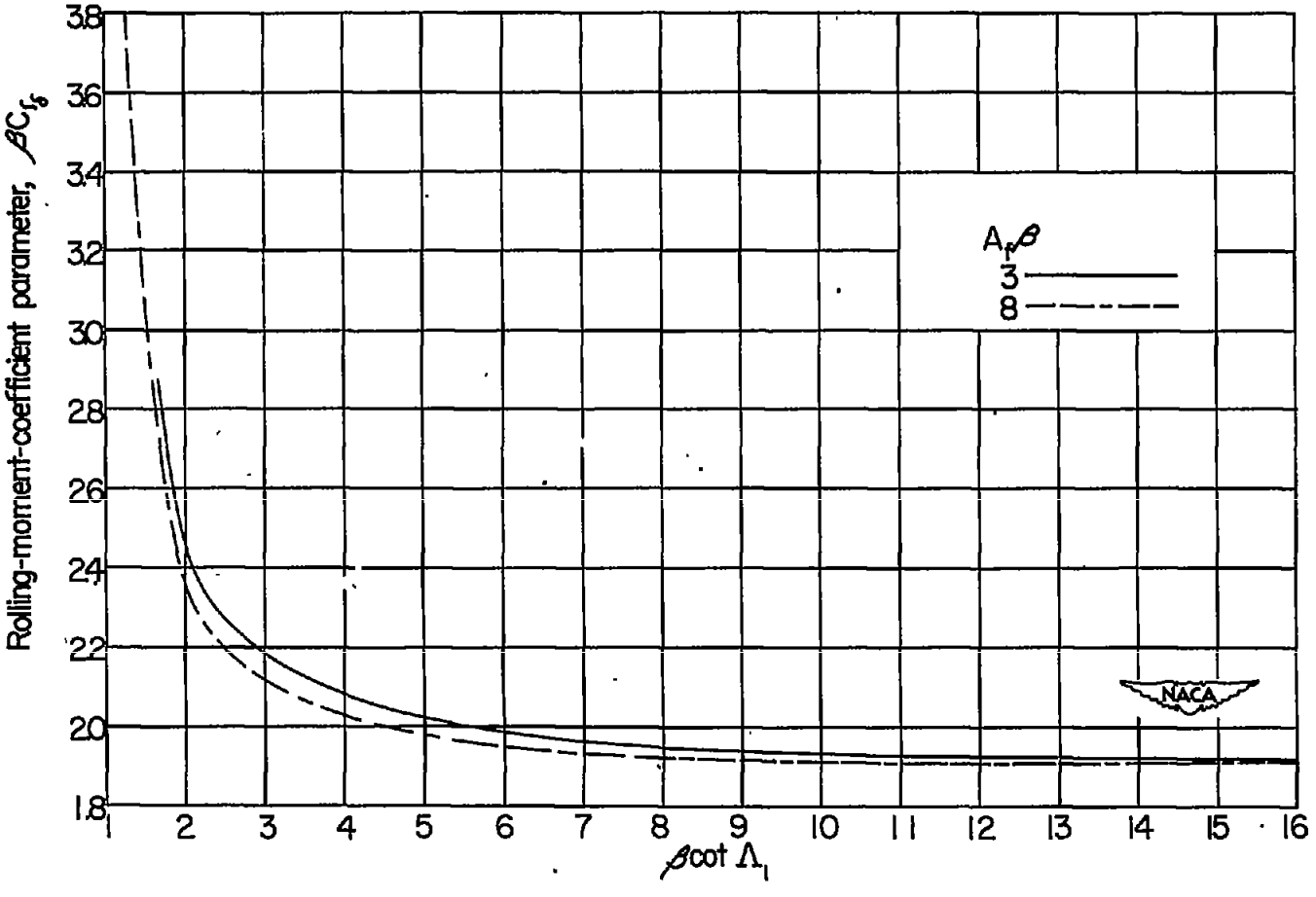

(b) $\lambda_f = 0.8$.

Figure 4.- Continued.

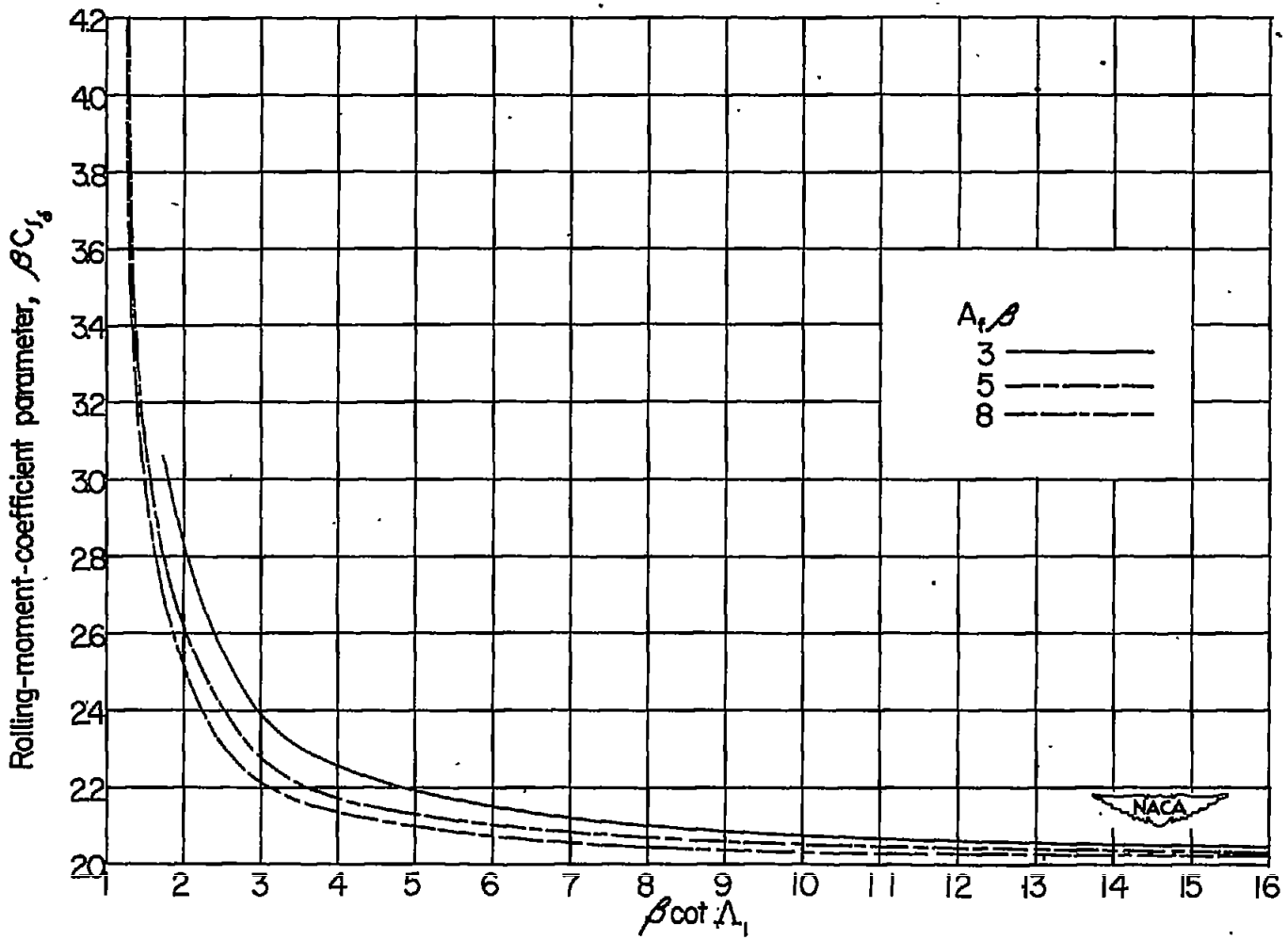

(c) $\lambda_f = 1.0$.

Figure 4.- Concluded.

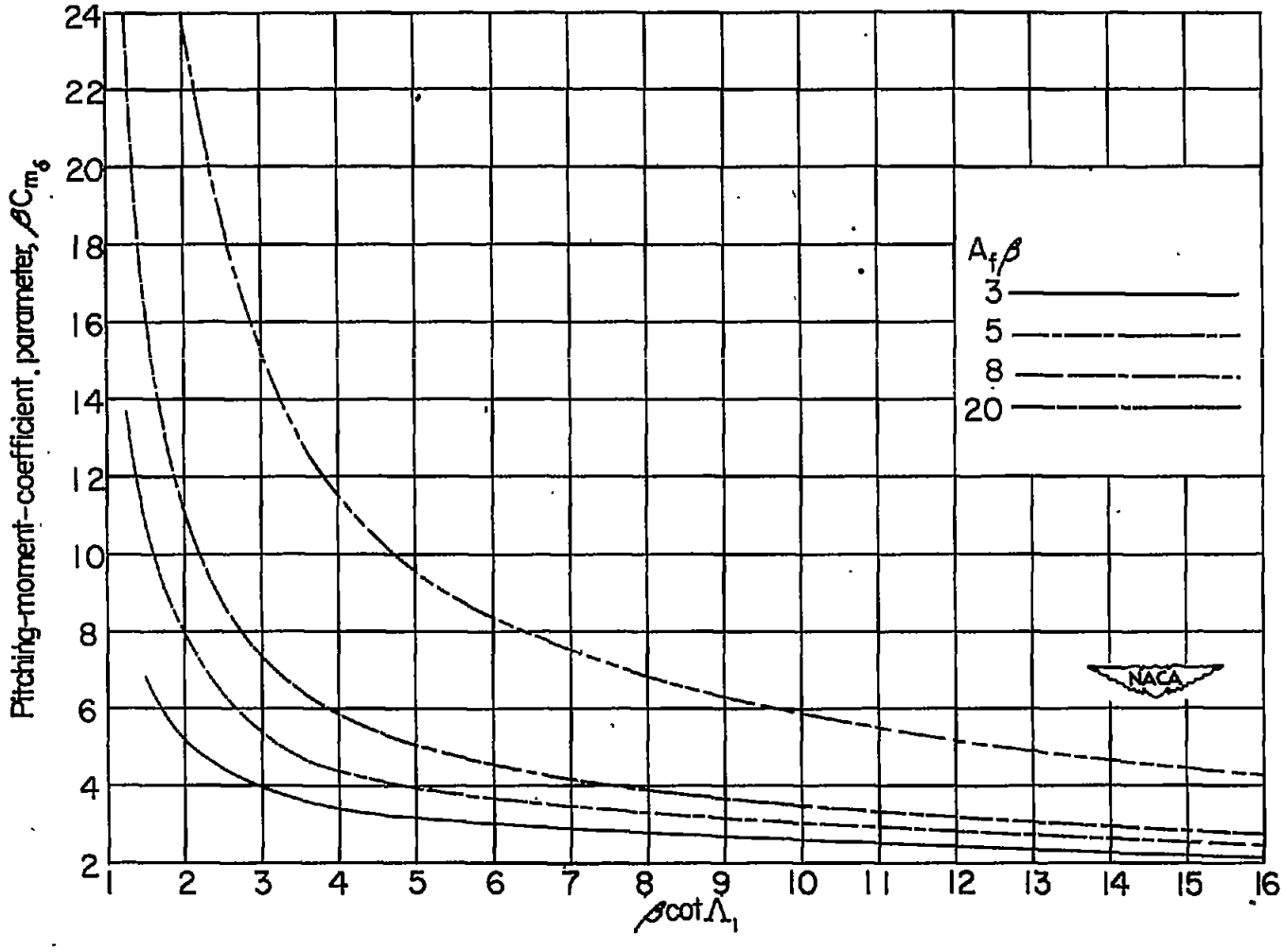

(a) $\lambda_f = 0.6$.

Figure 5.- Variation of βC_{m_δ} with $\beta \cot \Lambda_1$ for several families of $A_f\beta$ and λ_f.

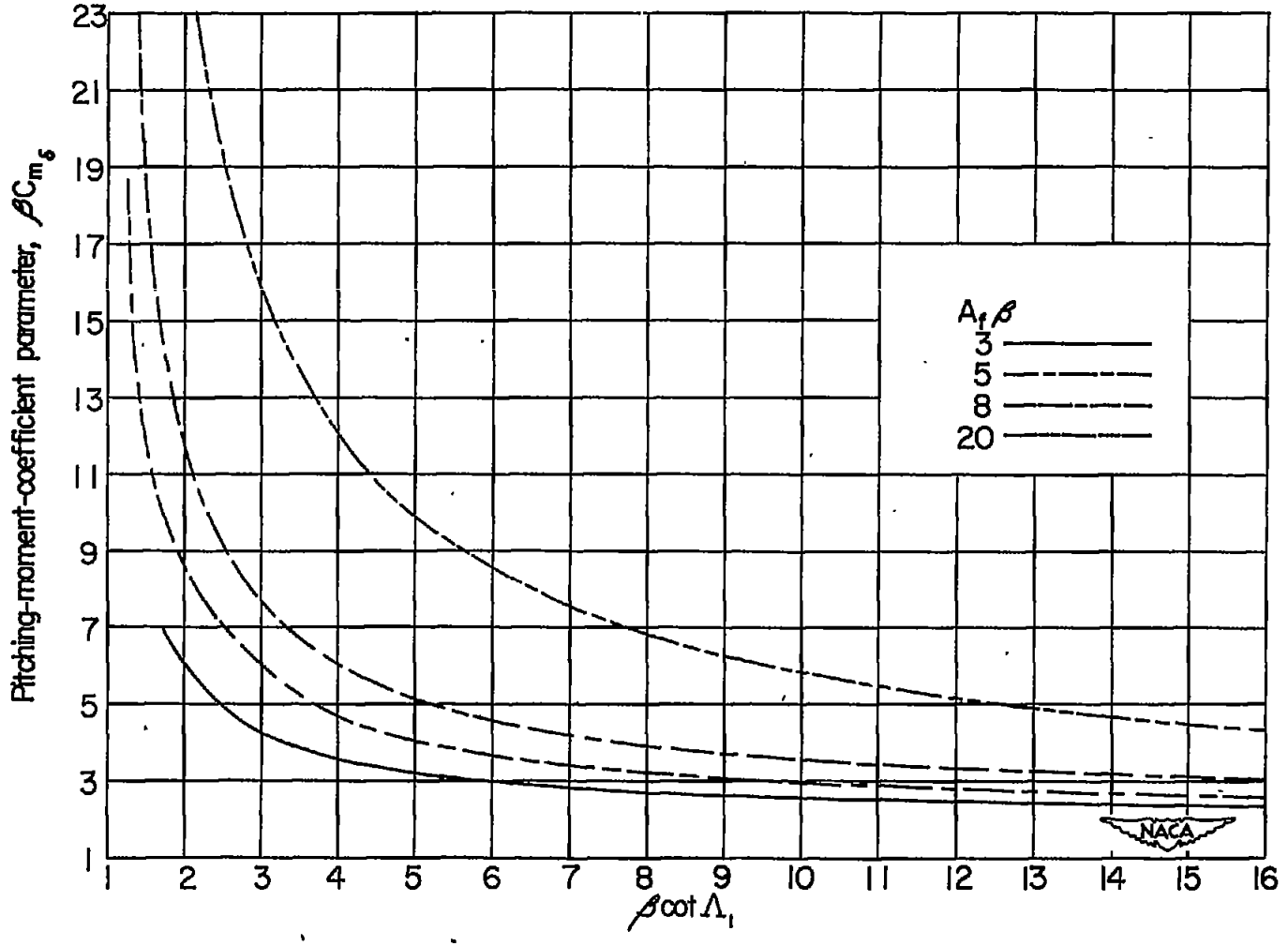

(b) $\lambda_f = 0.8$.

Figure 5.- Continued.

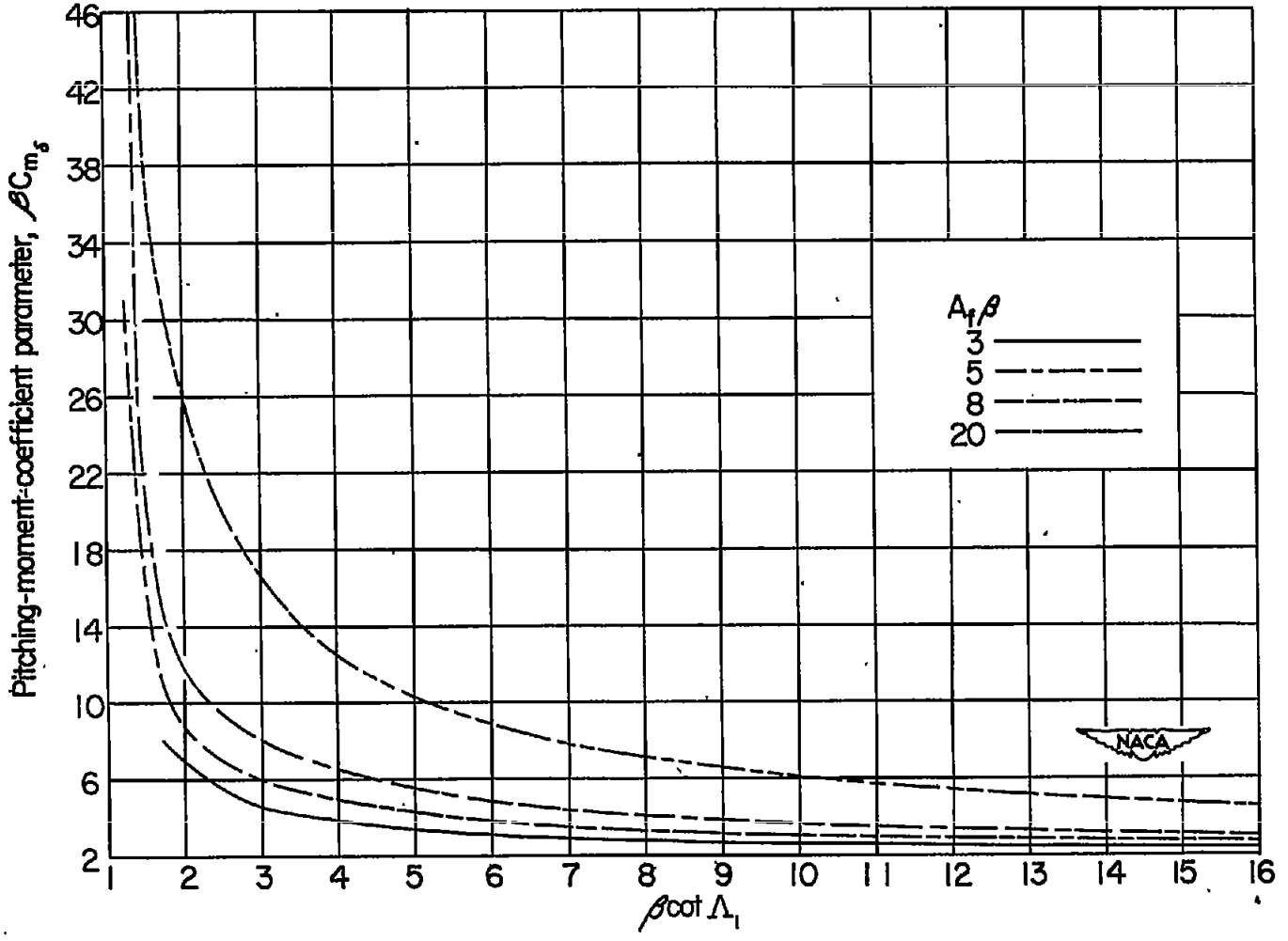

(c) $\lambda_f = 1.0$.

Figure 5.- Concluded.

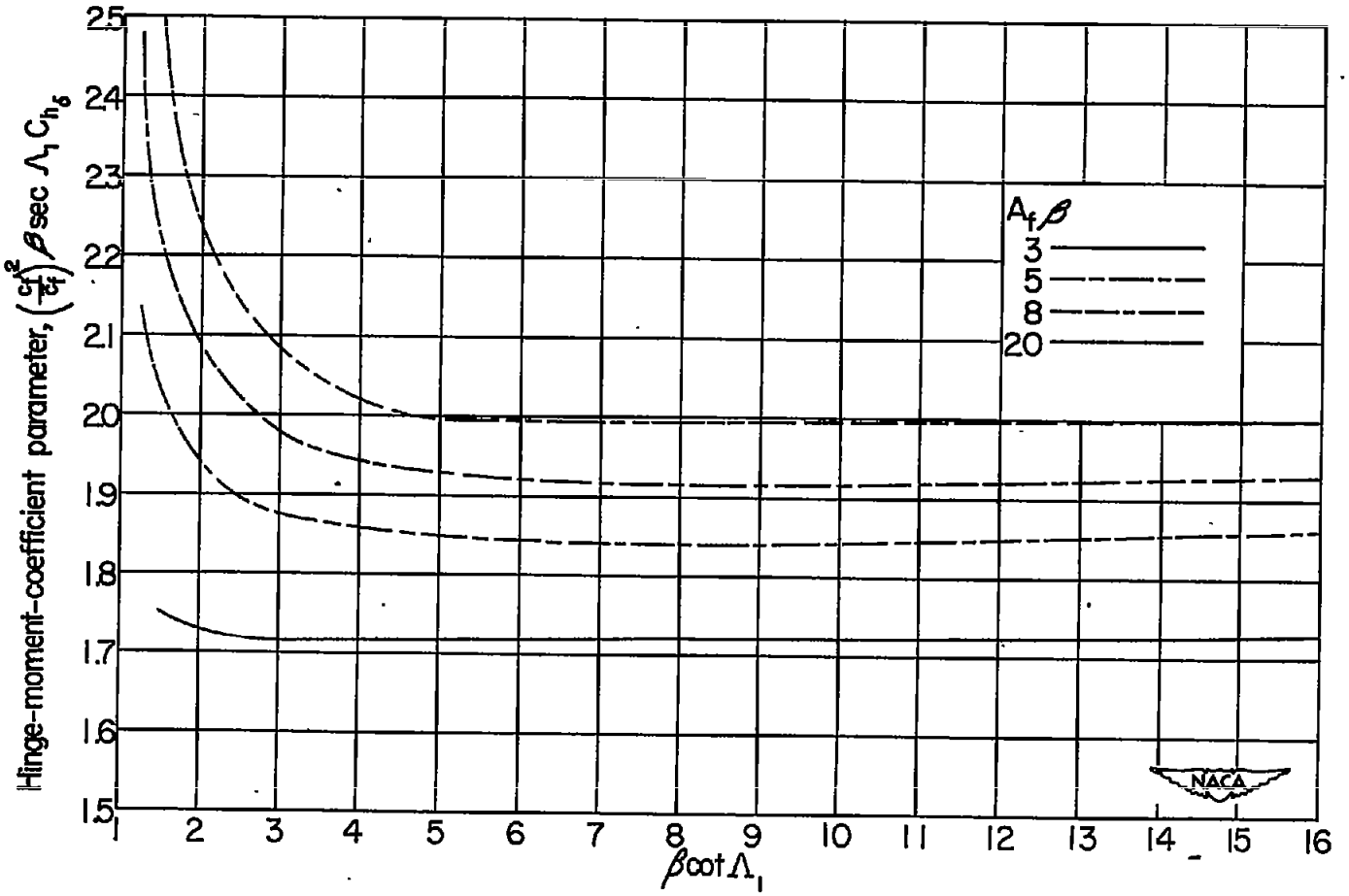

(a) $\lambda_f = 0.6$.

Figure 6.- Variation of $\left(\frac{c_f'}{c_f}\right)^2 \beta \sec \Lambda_1 C_{h_\delta}$ with $\beta \cot \Lambda_1$ for several families of $A_f\beta$ and λ_f.

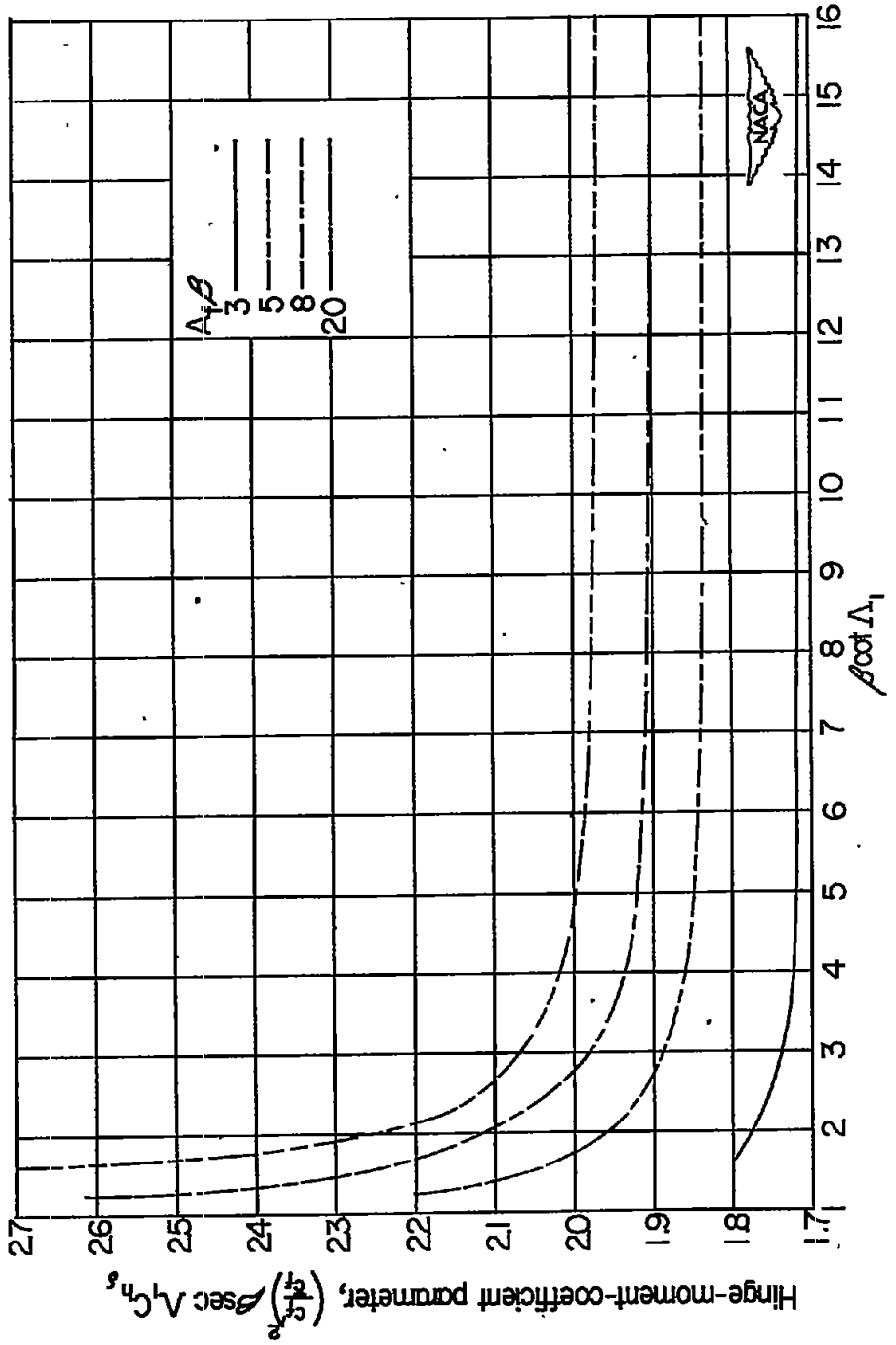

(b) $\lambda_1 = 0.8$.

Figure 6.- Continued.

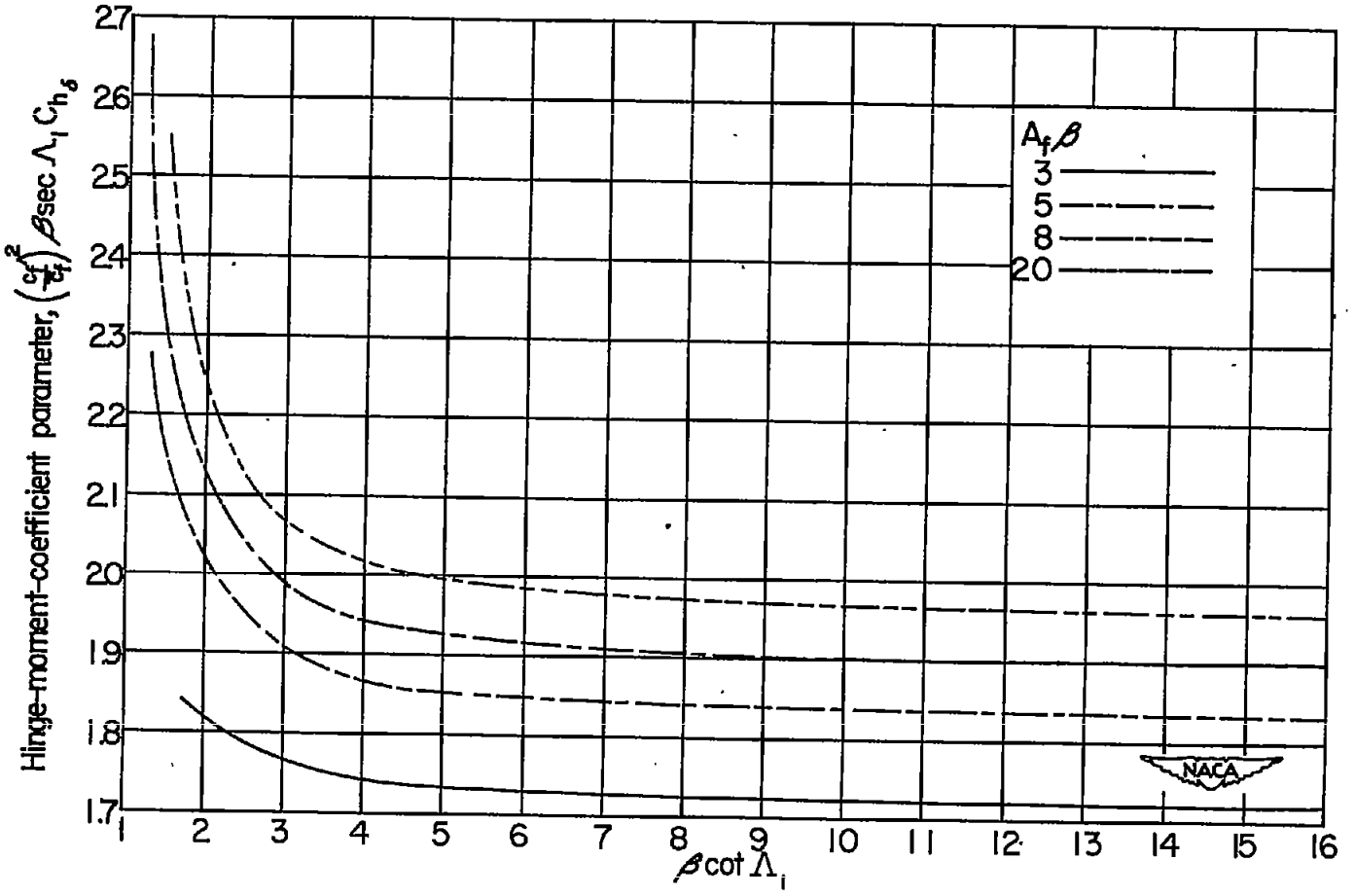

(c) $\lambda_f = 1.0$.

Figure 6.- Concluded.

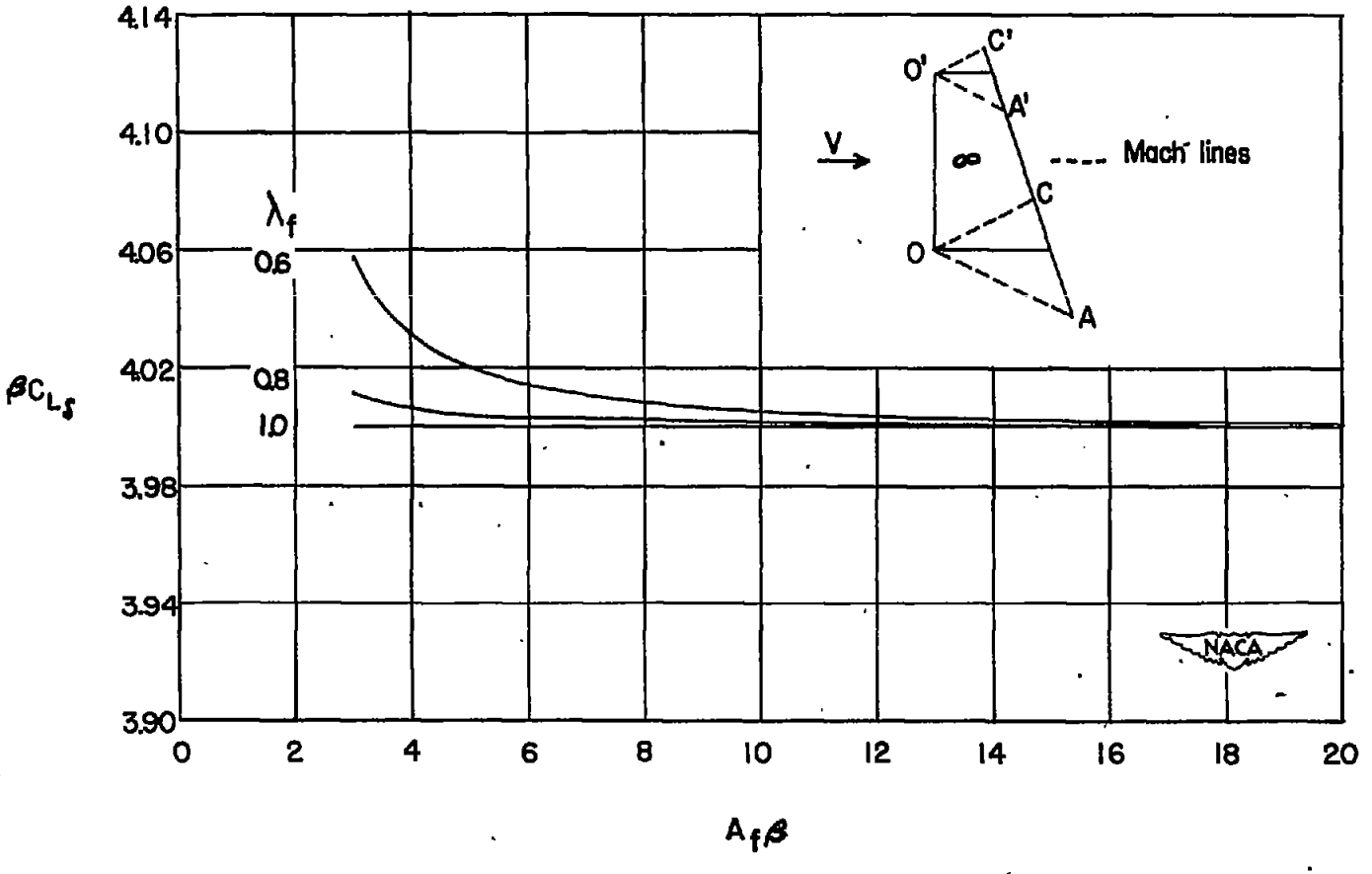

Figure 7.- Variation of βC_{L_δ} with $A_f\beta$ and λ_f for a control surface having an unswept leading edge.

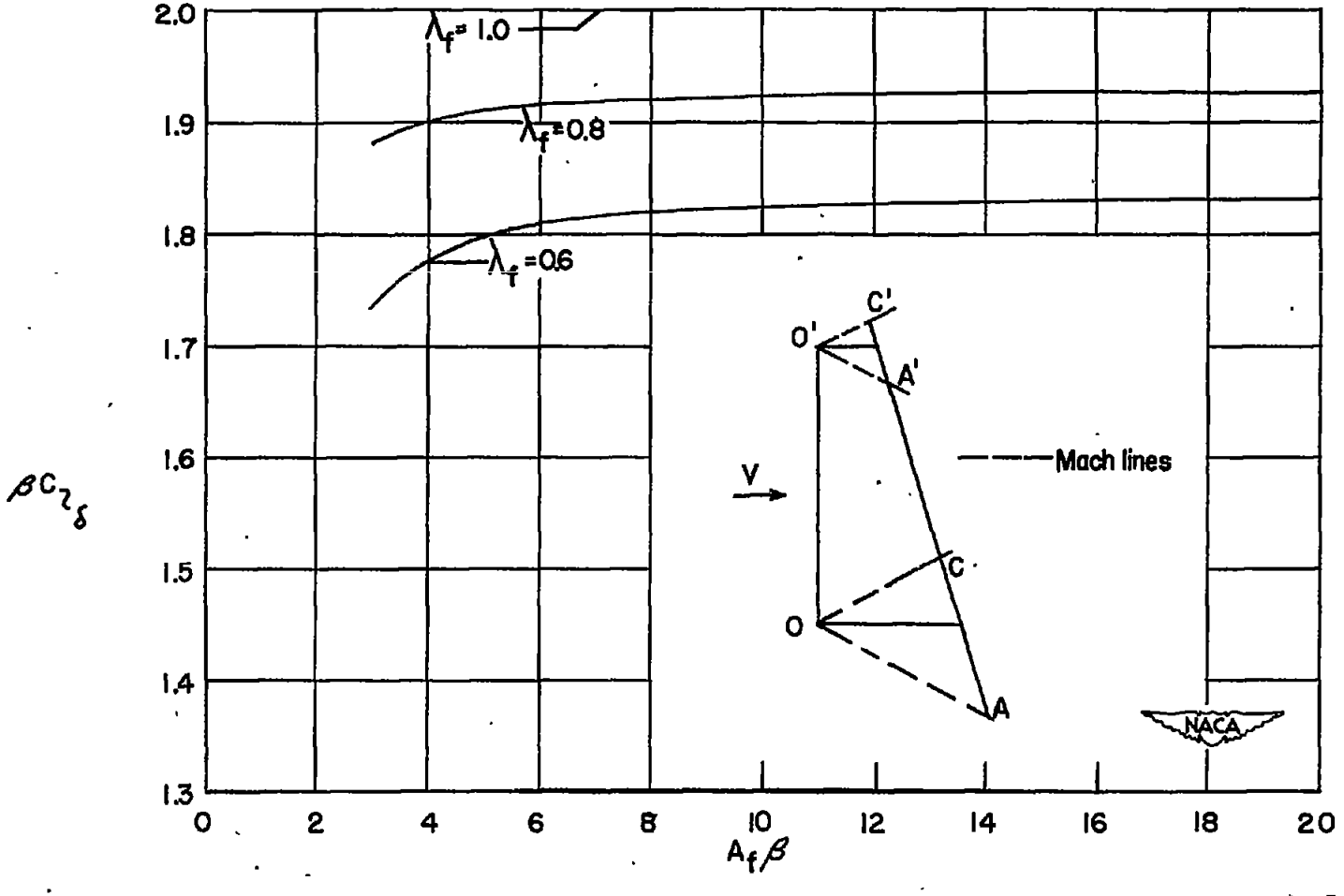

Figure 8.- Variation of βC_{l_δ} with $A_f\beta$ and λ_f for a control surface having an unswept leading edge.

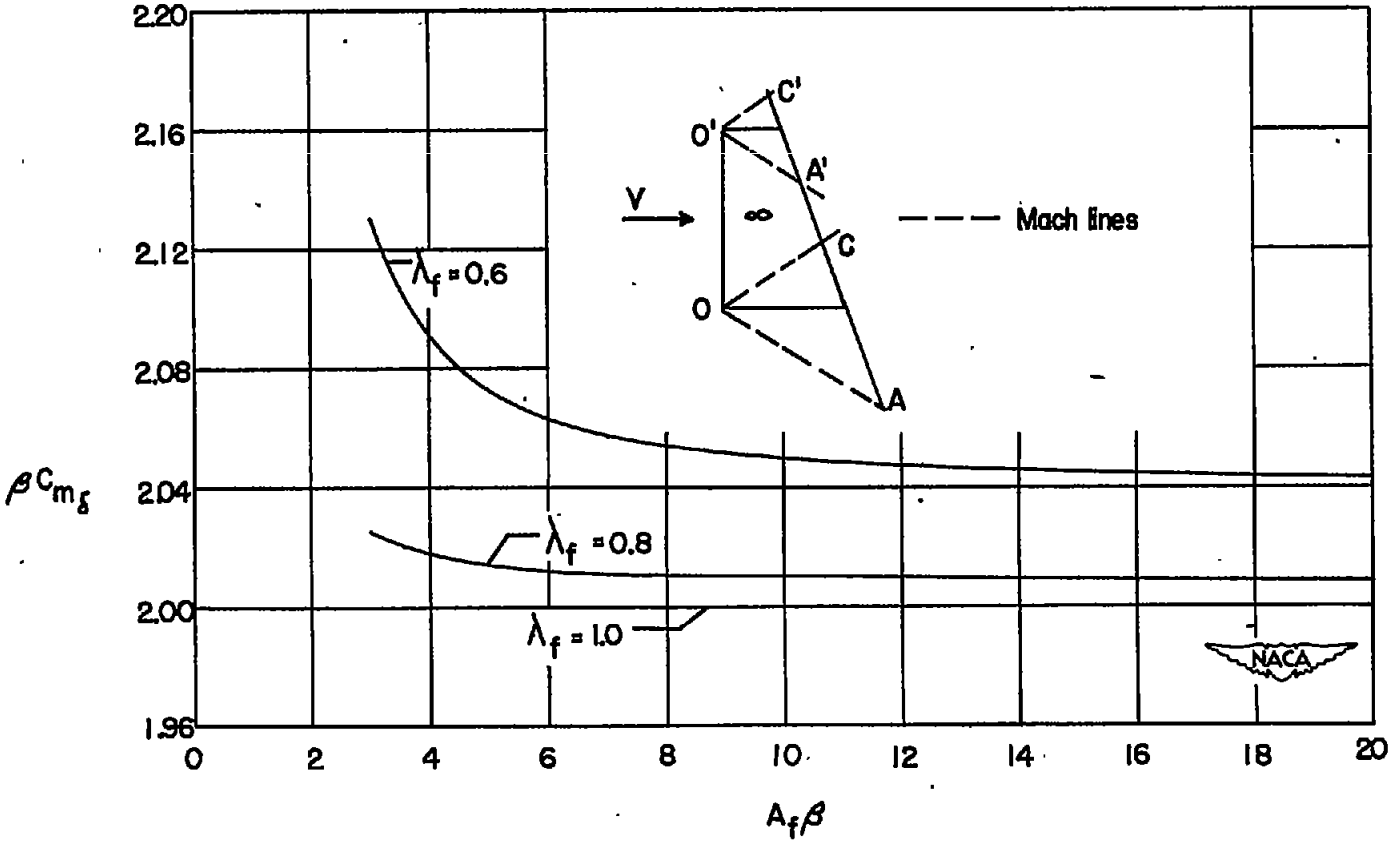

Figure 9.- Variation of βC_{m_δ} with $A_f\beta$ and λ_f for a control surface having an unswept leading edge.

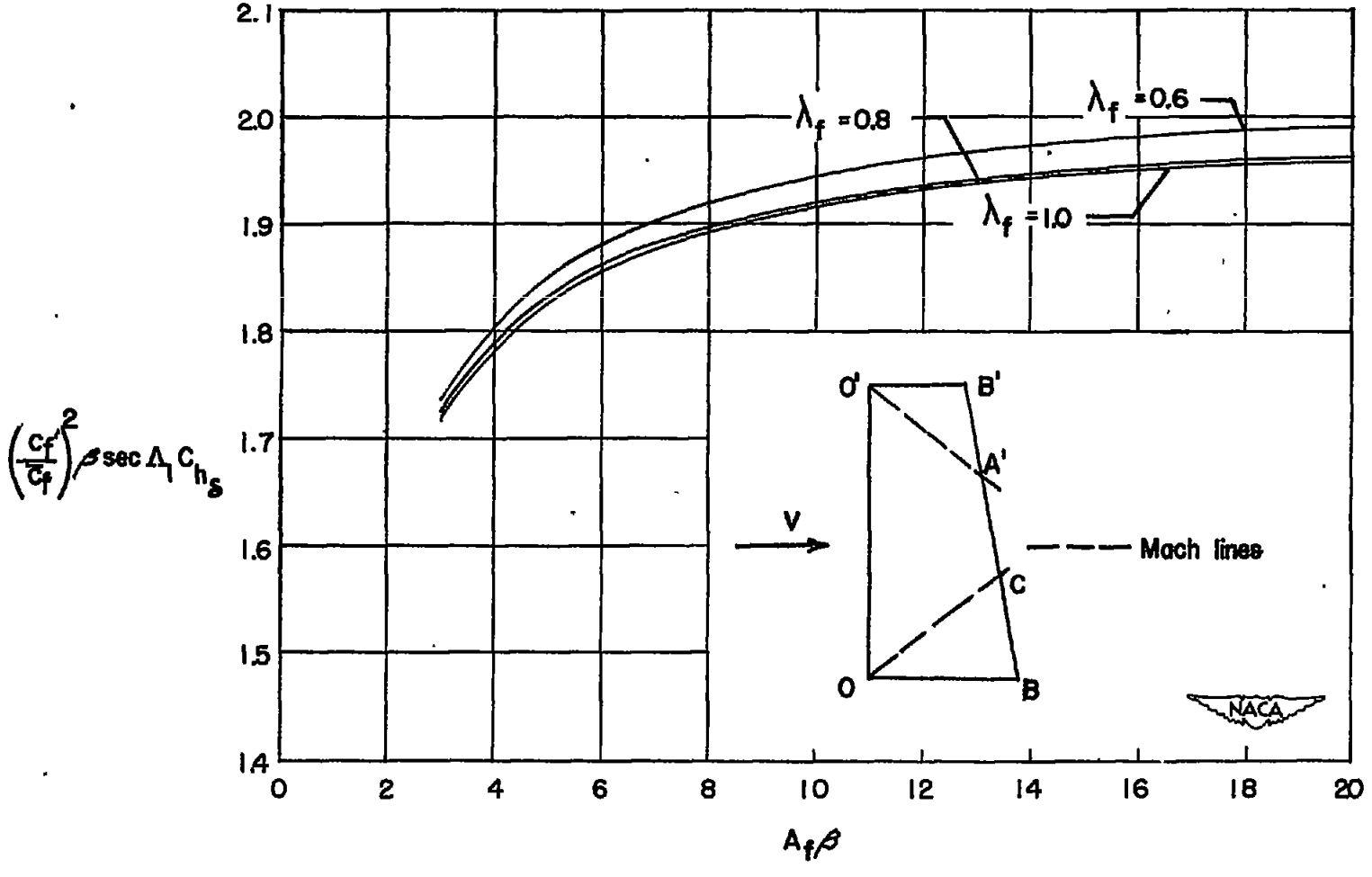

Figure 10.- Variation of $\left(\frac{c_f'}{c_f}\right)^2 \beta \sec \Lambda_1 C_{h_\delta}$ with $A_f\beta$ and λ_f for a control surface having an unswept leading edge.

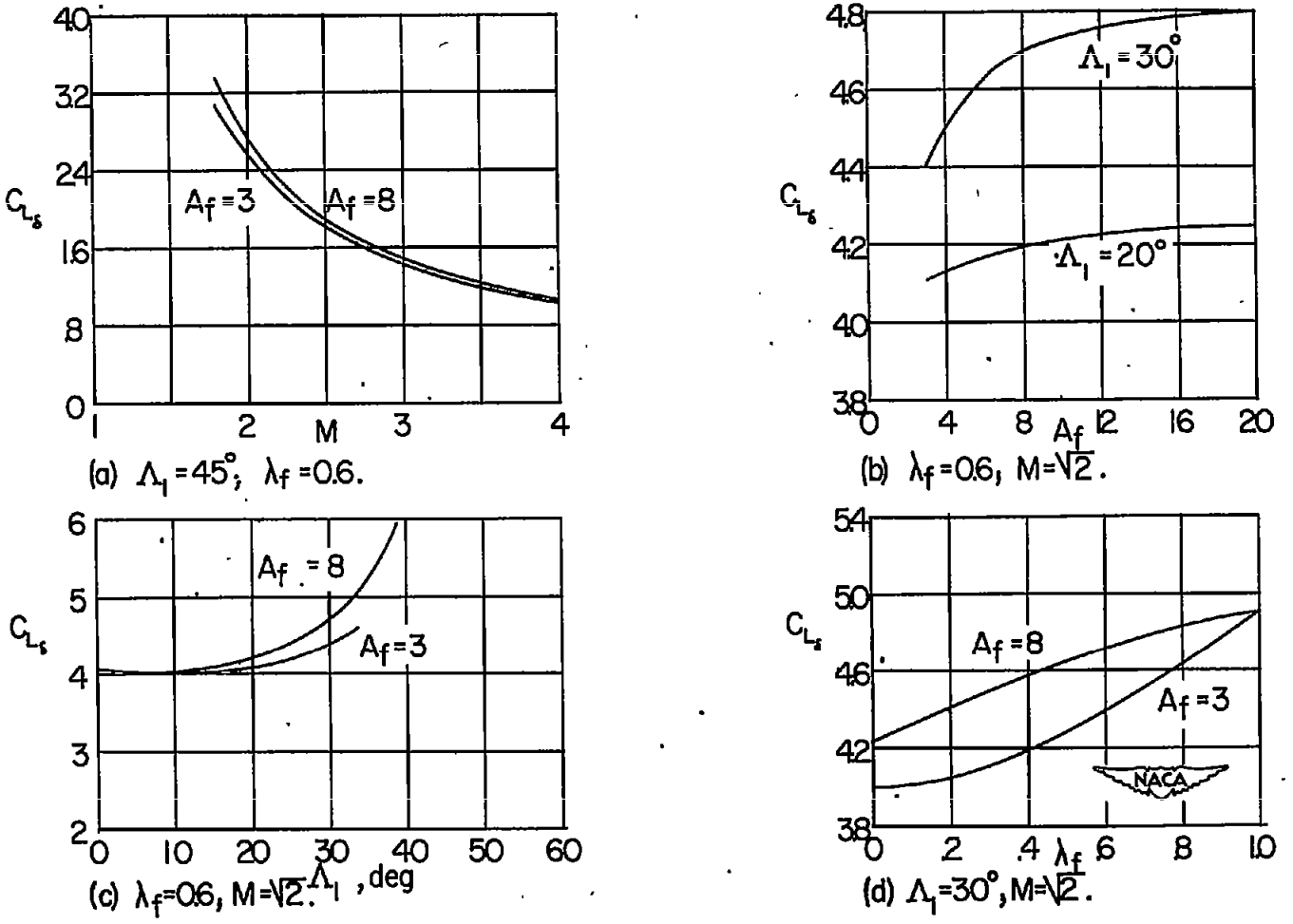

Figure 11.- Some illustrative variations in C_{L_δ} with Mach number, aspect ratio, leading-edge sweep, and taper ratio.

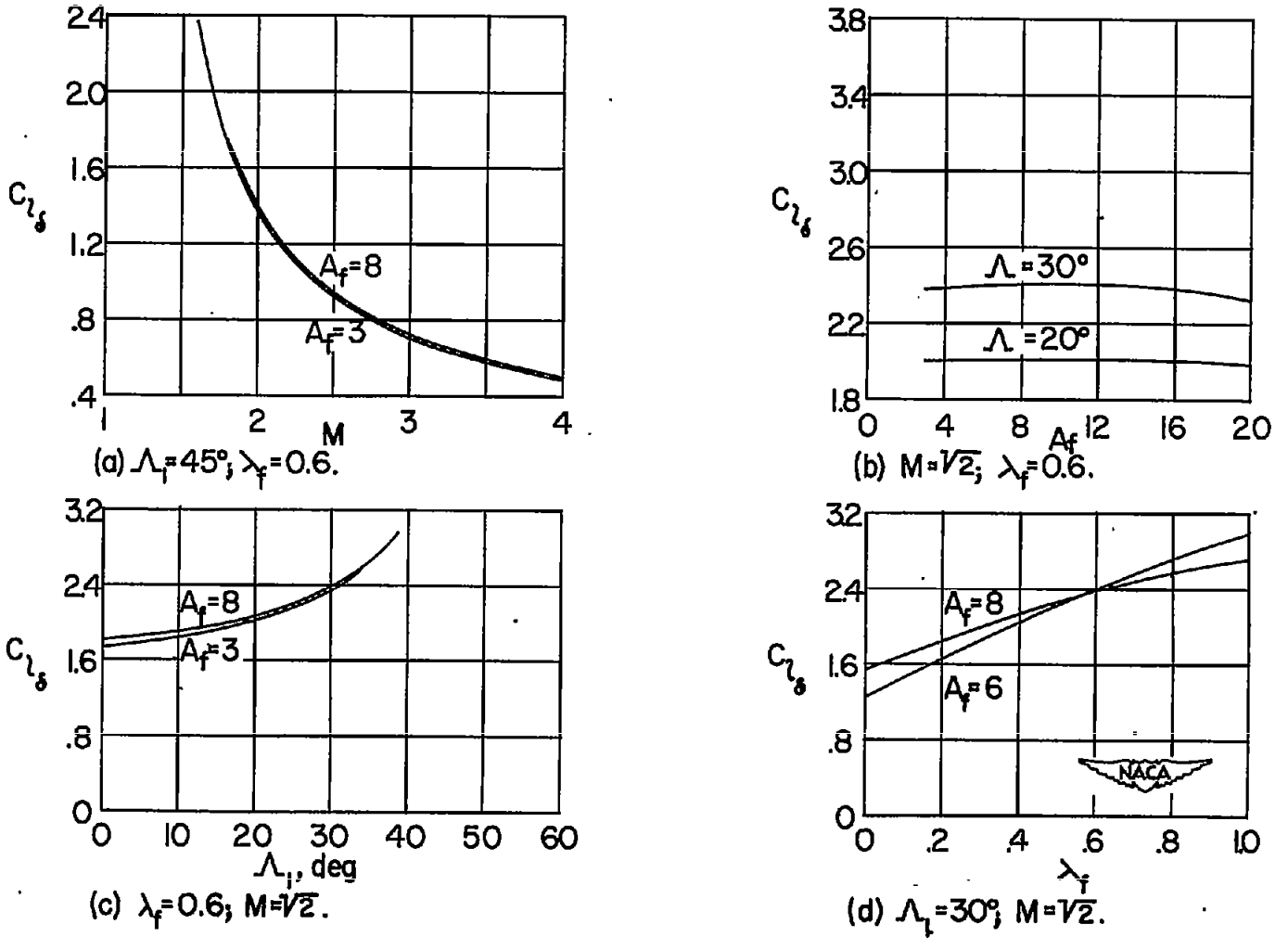

Figure 12.- Some illustrative variations in C_{l_δ} with Mach number, aspect ratio, leading-edge sweep, and taper ratio.

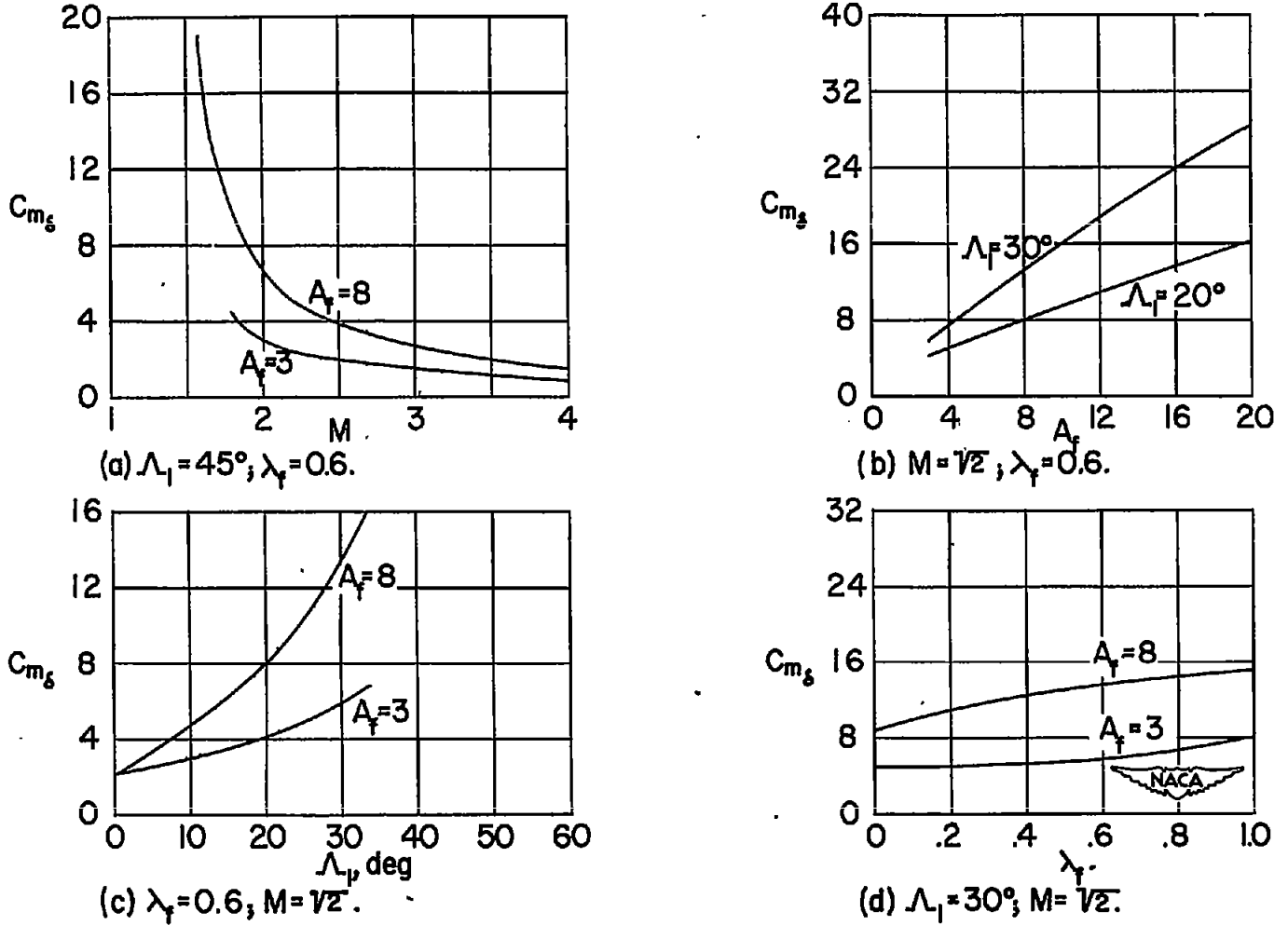

Figure 13.- Some illustrative variations in C_{m_δ} with Mach number, aspect ratio, leading-edge sweep, and taper ratio.

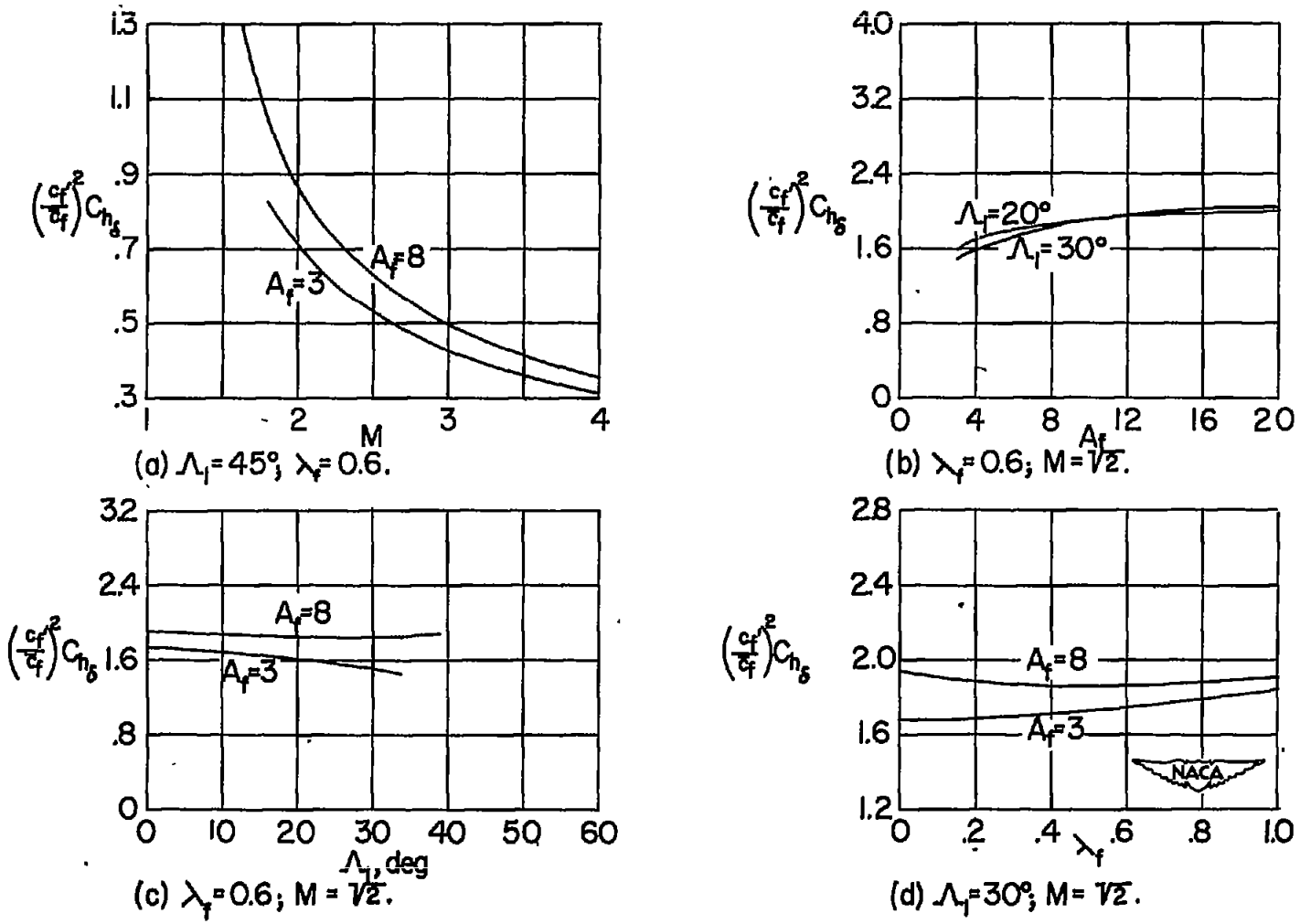

Figure 14.- Some illustrative variations in $\left(\frac{c_f'}{c_f}\right)^2 C_{h_\delta}$ with Mach number, aspect ratio, leading-edge sweep, and taper ratio.